JOURNAL OF MOLECULAR SPECTROSCOPY 163, 483–509 (1994)

Fourfold Clusters of Rovibrational Energy Levels for H_2S Studied with a Potential Energy Surface Derived from Experiment

IGOR N. KOZIN[1] AND PER JENSEN

Physikalisch-Chemisches Institut, Justus-Liebig-Universität Giessen, Heinrich-Buff-Ring 58, D-35392 Giessen, Germany

We report here an optimization of the parameters in an analytical representation of the potential energy function for the electronic ground state of hydrogen sulfide H_2S on the basis of experimental data. The calculations are carried out with the MORBID (Morse Oscillator Rigid Bender Internal Dynamics) computer program (P. Jensen, *J. Mol. Spectrosc.* **128,** 478–501, 1988; *J. Chem. Soc. Faraday Trans. 2* **84,** 1315–1340, 1988; *in* "Methods in Computational Molecular Physics" (S. Wilson and G. H. F. Diercksen, Eds.), Plenum, New York, 1992). In the least-squares fitting, we adjusted 14 parameters to fit a total of 548 rotation–vibration energy spacings involving $J \leqslant 5$ for the four isotopic molecules $H_2{}^{32}S$, $D_2{}^{32}S$, $HD^{32}S$, and $H_2{}^{34}S$. The data were reproduced with root-mean-square deviations of 0.134 cm^{-1} for the rotational energy spacings and 0.422 cm^{-1} for the vibrational spacings. We have used the fitted potential energy surface as the starting point for a theoretical investigation of the nearly degenerate, four-member groups of energy levels formed in the rotation–vibration energy spectrum of H_2S. Toward this end, we have calculated the rovibrational energy levels in the vibrational ground state, the ν_2 vibrational state, and the $\nu_1/\nu_3/2\nu_2$ interacting vibrational states of $H_2{}^{32}S$ for $J \leqslant 40$. The rotational energy level patterns obtained for these vibrational states of $H_2{}^{32}S$ are very similar in structure to those calculated previously for $H_2{}^{80}Se$ (P. Jensen and I. N. Kozin, *J. Mol. Spectrosc.* **160,** 39–57, 1993; I. N. Kozin and P. Jensen, *J. Mol. Spectrosc.* **161,** 186–207, 1993), although there is some difference in detail.

1. INTRODUCTION

In the traditional treatment of molecular rotation and vibration, it is assumed that the rotational energy levels are given essentially as those of a rigid rotor taken to be the molecule in its equilibrium configuration. The rotation–vibration interaction terms in the molecular Hamiltonian, which cause the rotational energy levels of the real molecule to differ from the rigid rotor levels, are treated as perturbations. It is known, however, that for some molecules rotation–vibration interaction leads to a qualitative change of the rotational energy level pattern relative to that of a rigid rotor. For example, it has been shown experimentally (*1–3*) that nearly degenerate, four-member groups of energy levels are formed in the vibrational ground state of the molecule H_2Se when the angular momentum quantum number J increases. Such clusters do not appear in the energy spectrum of a rigid rotor, and initially the phenomenon was investigated by means of semiclassical theory and simplified quantum mechanical models (*4–8*). Thus Zhilinskii and Pavlichenkov (*4*) first predicted the cluster formation in the vibrational ground state of the water molecule in a semiclassical study. More detailed discussions of the effect have been given by Makarewicz and Pyka (*5–*

[1] Present address: Applied Physics Institute, Russian Academy of Science, Uljanov Street 46, 603 600 Nizhnii Novgorod, Russia.

0022-2852/94 $6.00

7). The formation of fourfold rovibrational energy clusters in isolated vibrational states (see Refs. (*1–7*)) is probably the most surprising phenomenon in H_2X molecules. It can be satisfactorily explained by rigid bender-type models which neglect the stretching vibrational motion of the molecule but account explicitly for the bending motion (*4–7*). Another type of fourfold energy clusters in H_2X molecules was predicted by Lehmann (*8*) in model quantum mechanical calculations using a specially designed local mode effective Hamiltonian. These clusters appear when two stretching vibrational states of the molecule are nearly degenerate due to local mode effects.

In two recent papers (*9, 10*), we have reported realistic quantum mechanical calculations of cluster energies and wavefunctions in the vibrational ground state and the ν_1, ν_2, ν_3, and $2\nu_2$ states of H_2Se using the MORBID (Morse Oscillator Rigid Bender Internal Dynamics) Hamiltonian and computer program (*11–13*). As the initial step of that work, we determined the potential energy surface for the electronic ground state of H_2Se in a direct least-squares fitting to experimental data. We fitted a selection of 303 rotation–vibration energy spacings of $H_2{}^{80}Se$, $D_2{}^{80}Se$, and $HD^{80}Se$ involving $J \leq 5$ with a root-mean-square (RMS) deviation of 0.0975 cm^{-1} for the rotational energy spacings and 0.268 cm^{-1} for the vibrational spacings (*9*). The potential energy surface resulting from the fitting was used for investigating the cluster structures of the rotational energy levels in the vibrational ground state (*9*), in the three fundamental vibrational states, and in the $2\nu_2$ state (which is close to the ν_1 and ν_3 states) of $H_2{}^{80}Se$ (*10*). The results of these calculations can be summarized as follows:

(1) For the vibrational ground state of $H_2{}^{80}Se$, our calculation of the cluster structure, which has been observed experimentally up to $J = 23$ (*1–3*), is in good agreement with the experimental results [see Fig. 2 of Ref. (*9*)]. Further, we analyzed the wavefunctions for the cluster of highest energy in each J multiplet to show that of the four wavefunction components forming this cluster, two will have angular momentum projections of $-\hbar J$ and $\hbar J$, respectively, along a so-called *localization axis* A which lies approximately along one of the H–Se bonds (see Fig. 1), and the other two will have angular momentum projections of $-\hbar J$ and $\hbar J$, respectively, along the axis A' (Fig. 1) which can be obtained by subjecting A to a rotation around the C_2 symmetry

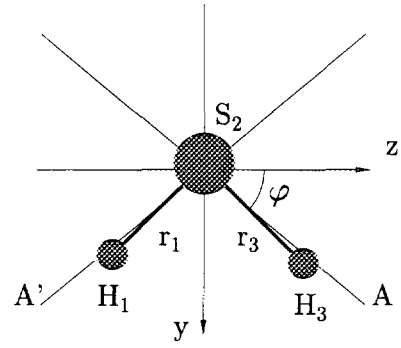

FIG. 1. The numbering of the nuclei and the molecule-fixed coordinate system used to describe the H_2S molecule in the MORBID approach. The molecule-fixed x axis is perpendicular to the plane of the molecule. The figure further shows the localization axes A and A' appropriate for the primitive cluster states (see text). The axis A forms the angle φ with the molecule-fixed z axis.

axis of the molecule in its equilibrium configuration. These results are in accordance with predictions from semiclassical theory.

(2) For the ν_2 and $2\nu_2$ states our calculations predict a cluster formation entirely analogous to that in the vibrational ground state. In the $2\nu_2$ state, the clusters are sometimes distorted by interactions with the ν_1 and ν_3 states.

(3) For the ν_1/ν_3 interacting vibrational states we found (*10*) that a "new" type of fourfold cluster arises through coalescence (with increasing J) of rotational energy doublets belonging to the ν_1 vibrational state with doublets belonging to the ν_3 state. In Ref. (*10*) we took credit for discovering this cluster type, but we subsequently have become aware of the work by Lehmann (*8*) mentioned above, in which he predicted the new clusters for vibrational levels of H_2Se with $v_1 + v_3 = 3$. The wavefunctions corresponding to the new cluster states are fifty-fifty mixtures of ν_1 and ν_3 basis states. We showed that when the small energy differences between individual cluster components are neglected, so that each cluster is represented by a four-dimensional space of degenerate eigenfunctions for the rotation–vibration Hamiltonian, we can find basis vectors in this space which give a simple picture of the molecular motion in a cluster state: The stretching excitation is localized in one of the bonds, and the molecule rotates around this bond.

The two types of energy clusters described above represent two different mechanisms for cluster formation. The analyses reported in Refs. (*4–8*) have been very useful for understanding the new phenomena, and the conclusions drawn from them agree with those from our work on the H_2Se molecule (*9, 10*). However, Refs. (*9, 10*) have shown that in order to obtain realistic predictions of the cluster effects it is necessary to consider all vibrational modes of the molecule. For example, we found that even though the appearance of fourfold energy clusters can be predicted from a rigid bender-type model neglecting the stretching vibrations (*4–7*), the details of the cluster structure are very significantly influenced by the stretching motion (*9, 10*). Hence approaches like MORBID, which account explicitly for all motions of the molecule, are necessary to obtain a satisfactory description of the cluster phenomenon.

The present paper reports an analysis of the cluster structure in the vibrational ground state and the ν_1, ν_2, ν_3, and $2\nu_2$ states of hydrogen sulfide H_2S, carried out in much the same way as the work on H_2Se described above. Below we see that the rotation–vibration energy spectrum of H_2S exhibits all the cluster effects already determined for H_2Se, but the cluster formation takes place at higher J values than those found for H_2Se so that it is less amenable to experimental observation. The paper is structured as follows: Section II describes a determination of the potential energy surface for the electronic ground state of H_2S by direct least-squares fitting to experimental data. In Section III, we describe an extensive calculation of the rotation–vibration energy levels in the vibrational ground state, the ν_2 vibrational state, and the $\nu_1/\nu_3/2\nu_2$ interacting vibrational states of $H_2{}^{32}S$ for $J \leqslant 40$. Section IV reports an analysis of the wavefunctions obtained from this calculation, and Section V offers conclusions.

II. THE FITTING

The fitting of the potential energy surface for H_2S described here was carried out with the MORBID computer program. This theoretical approach to calculating the rotation–vibration energies for a triatomic molecule directly from the potential energy

function has been extensively described in Refs. (*11–13*) and Ref. (*9*) gives a summary. We refer the reader to these publications for details. However, for completeness we give here the analytical representation of the potential energy function used in the present work,

$$V(\Delta r_1, \Delta r_3, \bar{\rho}) = V_0(\bar{\rho}) + \sum_j F_j(\bar{\rho}) y_j + \sum_{j \le k} F_{jk}(\bar{\rho}) y_j y_k + \sum_{j \le k \le m} F_{jkm}(\bar{\rho}) y_j y_k y_m + \sum_{j \le k \le m \le n} F_{jkmn}(\bar{\rho}) y_j y_k y_m y_n, \quad (1)$$

where all of the indices j, k, m, and n assume the values 1 or 3. The quantity y_j in Eq. (1) is given by

$$y_j = 1 - \exp(-a_j \Delta r_j), \quad (2)$$

where the a_j are molecular constants and $\Delta r_j = r_j - r_j^e$, $j = 1$ or 3, is defined as a displacement from the equilibrium value r_j^e of the distance r_j between the "outer" nucleus $j = 1$ or 3 and the "center" nucleus 2. The quantity $\bar{\rho}$ is the instantaneous value of the bond angle supplement (see Fig. 1 of Ref. (*11*)). The $F_{jkm}\ldots$ expansion coefficients of Eq. (1) are functions of $\bar{\rho}$ and defined as

$$F_j(\bar{\rho}) = \sum_{i=1}^{4} f_j^{(i)} (\cos \rho_e - \cos \bar{\rho})^i, \quad (3)$$

and

$$F_{jk}\ldots(\bar{\rho}) = f_{jk}^{(0)}\ldots + \sum_{i=1}^{N} f_{jk}^{(i)}\ldots (\cos \rho_e - \cos \bar{\rho})^i, \quad (4)$$

where ρ_e is the equilibrium value of $\bar{\rho}$ and the $f_{jk}^{(i)}\ldots$ are expansion coefficients. The function $F_{jk}(\bar{\rho})$ has $N = 3$, $F_{jkl}(\bar{\rho})$ has $N = 2$, and $F_{jklm}(\bar{\rho})$ has $N = 1$. The function $V_0(\bar{\rho})$ is the potential energy for the molecule bending with bond lengths fixed at their equilibrium values, and here we parameterize it as

$$V_0(\bar{\rho}) = \sum_{i=2}^{8} f_0^{(i)} (\cos \rho_e - \cos \bar{\rho})^i. \quad (5)$$

We aim at optimizing the parameters of Eqs. (1–5) in a least-squares fitting to experimental spectroscopic data for $H_2{}^{32}S$ and its isotopic species. Even though these molecules have been the subjects of many experimental studies during the past 40 years (*14–37*), only a rather limited number of vibrational states have been spectroscopically characterized. The highest excited vibrational states which have been investigated with present-day spectroscopic techniques are the (2, 1, 0) and (1, 1, 1) states of $H_2{}^{32}S$ (*36*) at 6288 and 6289 cm^{-1}, respectively. Vibrational term values have been measured for some higher excited states of $H_2{}^{32}S$ up to the (3, 1, 1) state at 11 009 cm^{-1} (*15*), but as these experimental values were obtained in 1956 they are probably of moderate precision. In addition to the data found in the literature (*14–37*), we used as input data for the fitting unpublished experimental term values kindly made available to us by Professor J.-M. Flaud (*38*).

In the construction of the input data points, we followed the strategy used in the water fitting of Ref. (*39*): we enter for each vibrational state the term value (relative to the $(v_1, v_2, v_3, J_{K_aK_c}) = (0, 0, 0, 0_{00})$ state of the isotopic molecule in question) of

the lowest measured rotation–vibration state together with the rotational spacings up to $J = 5$ (see Table I). For most of the vibrational states, which have been spectroscopically investigated, no experimentally derived rotation–vibration term values are directly given in the literature. For these states, we calculated such term values from the published rotation–vibration constants. The input data for the fitting consist mainly of energy spacings for $H_2{}^{32}S$ and its deuterated isotopomers $D_2{}^{32}S$ and $HD^{32}S$. In addition to these data, we included the known vibrational spacings for $H_2{}^{34}S$ (*32, 35, 36*) only. Even though some data for $H_2{}^{33}S$ are available (*28*), we did not use them in the fitting since owing to the small relative mass difference between the sulphur isotopes, we do not expect that the inclusion of such data will supply information not already present in the $H_2{}^{32}S$ data. The input data set used for the fitting comprised a total of 548 data points.

In the energy calculations carried out during the least-squares fitting, we used the following basis sets:

(1) For $H_2{}^{32}S$, we calculated the vibrational ($J = 0$) energy spacings with a basis set in which the stretching problem was prediagonalized [see Ref. (*11*)] with Morse oscillator functions $|n_1 n_3\rangle$ having $n_1 + n_3 \leq N_{\text{Stretch}} = 12$. In constructing the final rotation–vibration matrices we used the $N_{\text{Bend}} = 17$ lowest bending basis functions, the $N_A = 25$ lowest stretching basis functions of A_1 symmetry and the $N_B = 20$ lowest stretching basis functions of B_2 symmetry. The rotational spacings were calculated with a basis set having $N_{\text{Stretch}} = 10$, $N_{\text{Bend}} = 11$, and $(N_A, N_B) = (12, 9)$.

(2) For $D_2{}^{32}S$, the vibrational energy spacings were calculated with a basis set defined by $N_{\text{Stretch}} = 10$, $N_{\text{Bend}} = 11$, and $(N_A, N_B) = (12, 9)$. The basis set used for the rotational spacings had $N_{\text{Stretch}} = 9$, $N_{\text{Bend}} = 9$, and $(N_A, N_B) = (9, 6)$.

(3) For $HD^{32}S$, we calculated the rotation–vibration spacings used as input with the basis set $N_{\text{Stretch}} = 10$, $N_{\text{Bend}} = 9$, and $N_A = 10$.

(4) Finally, for $H_2{}^{34}S$, the vibrational energy spacings were calculated with a basis set defined by $N_{\text{Stretch}} = 10$, $N_{\text{Bend}} = 13$, and $(N_A, N_B) = (16, 12)$.

In order to start the iterative nonlinear least-squares fitting procedure we need initial guesses for the values of the parameters in Eqs. (1)–(5). Following the procedure described for H_2Se in Ref. (*9*), we determined such values on the basis of the results obtained by Kauppi and Halonen (*40*) in a least-squares fitting to rotation–vibration energy spacings for H_2S using a drastically simplified model. In the MORBID fitting, we could usefully vary 14 parameters. No parameters were constrained. The input data were reproduced with an RMS deviation of 0.134 cm^{-1} for the rotational energy spacings and 0.422 cm^{-1} for the vibrational spacings. Table I gives the complete input data set with residuals (obs − calc) and weights. The fitted parameter values are presented in Table II.

From the analytical expressions given in Eqs. (1)–(4) and the parameter values of Table II we have obtained values for the conventional "force constants" of H_2S, defined as the derivatives of $V(\Delta r_1, \Delta r_3, \bar{\rho})$ [Eq. (1)] at equilibrium, e.g.,

$$f_{rr} = \left(\frac{\partial^2 V}{\partial \Delta r_1^2}\right)_e, \tag{6}$$

$$f_{r\alpha} = \left(\frac{\partial^2 V}{\partial \Delta r_1 \partial \alpha}\right)_e, \tag{7}$$

etc., $\alpha = \pi - \bar{\rho}$ being the bond angle. The resulting values are given in Table III which

TABLE I

Observed and Calculated Vibrational and Rotational Term Values (cm^{-1}) for Hydrogen Sulfide

(v_1, v_2, v_3)	$J'_{K'_a K'_c} - J''_{K''_a K''_c}$	obs.[a] cm^{-1}	o.−c. cm^{-1}	weight	(v_1, v_2, v_3)	$J'_{K'_a K'_c} - J''_{K''_a K''_c}$	obs.[a] cm^{-1}	o.−c. cm^{-1}	weight
$H_2{}^{32}S$									
(0,0,0)[b]	0_{00}	0.0			(0,2,0)[d]	$2_{21}-0_{00}$	58.4666	0.0180	10.0
	$1_{01}-0_{00}$	13.74631	0.00043	100.0		$2_{20}-0_{00}$	61.9889	0.0444	10.0
	$1_{11}-0_{00}$	15.09011	0.00028	100.0		$3_{03}-0_{00}$	72.0145	0.0844	10.0
	$1_{10}-0_{00}$	19.37563	0.00061	100.0		$3_{13}-0_{00}$	72.0745	0.0815	10.0
	$2_{02}-0_{00}$	38.01607	0.00098	100.0		$3_{12}-0_{00}$	98.8268	0.1409	10.0
	$2_{12}-0_{00}$	38.29775	0.00078	100.0		$3_{22}-0_{00}$	100.6108	0.0943	10.0
	$2_{11}-0_{00}$	51.14016	0.00153	100.0		$3_{21}-0_{00}$	112.7911	0.1599	10.0
	$2_{21}-0_{00}$	55.16158	0.00170	100.0		$3_{31}-0_{00}$	122.6640	0.0342	10.0
	$2_{20}-0_{00}$	58.36884	0.00175	100.0		$3_{30}-0_{00}$	124.8276	0.0633	10.0
	$3_{03}-0_{00}$	71.42426	0.00172	100.0		$4_{04}-0_{00}$	114.4853	0.1350	10.0
	$3_{13}-0_{00}$	71.46515	0.00164	100.0		$4_{14}-0_{00}$	114.4939	0.1344	10.0
	$3_{12}-0_{00}$	95.05630	0.00299	100.0		$4_{13}-0_{00}$	153.1725	0.1941	10.0
	$3_{22}-0_{00}$	96.39246	0.00264	100.0		$4_{23}-0_{00}$	153.5773	0.1763	10.0
	$3_{21}-0_{00}$	107.36820	0.00221	100.0		$4_{22}-0_{00}$	178.1308	0.2659	10.0
	$3_{31}-0_{00}$	115.34059	0.00448	100.0		$4_{32}-0_{00}$	182.9107	0.1531	10.0
	$3_{30}-0_{00}$	117.39199	0.00386	100.0		$4_{31}-0_{00}$	192.2964	0.2383	10.0
	$4_{04}-0_{00}$	114.17217	0.00291	100.0		$4_{41}-0_{00}$	208.3298	0.0467	10.0
	$4_{14}-0_{00}$	114.17758	0.00289	100.0		$4_{40}-0_{00}$	209.4771	0.0690	10.0
	$4_{13}-0_{00}$	148.14058	0.00503	100.0		$5_{05}-0_{00}$	166.1306	0.2017	10.0
	$4_{23}-0_{00}$	148.41831	0.00472	100.0		$5_{15}-0_{00}$	166.1316	0.2013	10.0
	$4_{22}-0_{00}$	170.33574	0.00357	100.0		$5_{14}-0_{00}$	216.1626	0.2734	10.0
	$4_{32}-0_{00}$	173.96726	0.00434	100.0		$5_{24}-0_{00}$	216.2382	0.2687	10.0
	$4_{31}-0_{00}$	182.64849	0.00176	100.0		$5_{23}-0_{00}$	253.6457	0.3413	10.0
	$4_{41}-0_{00}$	195.66142	0.00977	100.0		$5_{33}-0_{00}$	255.1548	0.2799	10.0
	$4_{40}-0_{00}$	196.80212	0.00851	100.0		$5_{32}-0_{00}$	276.4300	0.4059	10.0
	$5_{05}-0_{00}$	166.34345	0.00465	100.0		$5_{42}-0_{00}$	285.9776	0.2051	10.0
	$5_{15}-0_{00}$	166.34417	0.00465	100.0		$5_{41}-0_{00}$	292.4622	0.2965	10.0
	$5_{14}-0_{00}$	210.21727	0.00809	100.0		$5_{51}-0_{00}$	315.3971	0.0537	10.0
	$5_{24}-0_{00}$	210.26477	0.00796	100.0		$5_{50}-0_{00}$	315.9475	0.0675	10.0
	$5_{23}-0_{00}$	243.34344	0.00655	100.0	(1,0,0)[d]	0_{00}	2614.4074	−0.2541	10.0
	$5_{33}-0_{00}$	244.39250	0.00638	100.0		$1_{01}-0_{00}$	13.5500	−0.0265	10.0
	$5_{32}-0_{00}$	263.73895	0.00073	100.0		$1_{11}-0_{00}$	14.8604	0.0051	10.0
	$5_{42}-0_{00}$	271.10604	0.00586	100.0		$1_{10}-0_{00}$	19.0928	−0.0132	10.0
	$5_{41}-0_{00}$	277.33758	0.00028	100.0		$2_{02}-0_{00}$	37.4603	−0.0428	10.0
	$5_{51}-0_{00}$	296.10442	0.01949	100.0		$2_{12}-0_{00}$	37.7267	−0.0301	10.0
	$5_{50}-0_{00}$	296.67760	0.01799	100.0		$2_{11}-0_{00}$	50.4016	−0.0865	10.0
(0,1,0)[c]	0_{00}	1182.5742	0.1361	10.0		$2_{21}-0_{00}$	54.3176	0.0093	10.0
	$1_{01}-0_{00}$	13.89027	0.01227	10.0		$2_{20}-0_{00}$	57.5514	−0.0233	10.0
	$1_{11}-0_{00}$	15.39011	0.00472	10.0		$3_{03}-0_{00}$	70.3701	−0.0661	10.0
	$1_{10}-0_{00}$	19.94299	0.01118	10.0		$3_{13}-0_{00}$	70.4066	−0.0636	10.0
	$2_{02}-0_{00}$	38.29127	0.02657	10.0		$3_{12}-0_{00}$	93.6816	−0.1274	10.0
	$2_{12}-0_{00}$	38.61890	0.02282	10.0		$3_{22}-0_{00}$	94.9421	−0.0730	10.0
	$2_{11}-0_{00}$	52.26090	0.04188	10.0		$3_{21}-0_{00}$	105.8151	−0.1678	10.0
	$2_{21}-0_{00}$	56.74698	0.01993	10.0		$3_{31}-0_{00}$	113.5128	0.0192	10.0
	$2_{20}-0_{00}$	60.10843	0.02980	10.0		$3_{30}-0_{00}$	115.8173	−0.0072	10.0
	$3_{03}-0_{00}$	71.68663	0.04699	10.0		$4_{04}-0_{00}$	112.4829	−0.1014	10.0
	$3_{13}-0_{00}$	71.73630	0.04601	10.0		$4_{14}-0_{00}$	112.4863	−0.1021	10.0
	$3_{12}-0_{00}$	96.86389	0.07282	10.0		$4_{13}-0_{00}$	145.9687	−0.1534	10.0
	$3_{22}-0_{00}$	98.41076	0.05665	10.0		$4_{23}-0_{00}$	146.2157	−0.1380	10.0
	$3_{21}-0_{00}$	109.97559	0.08152	10.0		$4_{22}-0_{00}$	167.8817	−0.2618	10.0
	$3_{31}-0_{00}$	118.85823	0.04058	10.0		$4_{32}-0_{00}$	171.3030	−0.1226	10.0
	$3_{30}-0_{00}$	120.96499	0.05090	10.0		$4_{31}-0_{00}$	180.0243	−0.2530	10.0
	$4_{04}-0_{00}$	114.28395	0.07571	10.0		$4_{41}-0_{00}$	191.9318	0.0014	10.0
	$4_{14}-0_{00}$	114.29081	0.07551	10.0		$4_{40}-0_{00}$	194.2170	0.0398	10.0
	$4_{13}-0_{00}$	150.54258	0.10555	10.0		$5_{05}-0_{00}$	163.8801	−0.1453	10.0
	$4_{23}-0_{00}$	150.87871	0.09937	10.0		$5_{15}-0_{00}$	163.8806	−0.1453	10.0
	$4_{22}-0_{00}$	174.08437	0.13372	10.0		$5_{14}-0_{00}$	207.1167	−0.1985	10.0
	$4_{32}-0_{00}$	178.25909	0.09530	10.0		$5_{24}-0_{00}$	207.1554	−0.1959	10.0
	$4_{31}-0_{00}$	187.28845	0.12502	10.0		$5_{23}-0_{00}$	239.8036	−0.2901	10.0
	$4_{41}-0_{00}$	201.75232	0.06558	10.0		$5_{33}-0_{00}$	240.7397	−0.2323	10.0
	$4_{40}-0_{00}$	202.89606	0.07307	10.0		$5_{32}-0_{00}$	259.9379	−0.4324	10.0
	$5_{05}-0_{00}$	166.17962	0.11262	10.0		$5_{42}-0_{00}$	266.7874	−0.1730	10.0
	$5_{15}-0_{00}$	166.18057	0.11258	10.0		$5_{41}-0_{00}$	273.4129	−0.3179	10.0
	$5_{14}-0_{00}$	213.04086	0.15138	10.0		$5_{51}-0_{00}$	292.6414	0.1502	10.0
	$5_{24}-0_{00}$	213.10089	0.14971	10.0		$5_{50}-0_{00}$	292.7896	0.1139	10.0
	$5_{23}-0_{00}$	248.29024	0.17925	10.0	(0,0,1)[d]	0_{00}	2628.4552	−0.1001	10.0
	$5_{33}-0_{00}$	249.55181	0.15829	10.0		$1_{01}-0_{00}$	13.6136	−0.0026	10.0
	$5_{32}-0_{00}$	269.84893	0.20124	10.0		$1_{11}-0_{00}$	14.8215	−0.0368	10.0
	$5_{42}-0_{00}$	278.25270	0.13454	10.0		$1_{10}-0_{00}$	19.0782	−0.0268	10.0
	$5_{41}-0_{00}$	284.61247	0.16465	10.0		$2_{02}-0_{00}$	37.5538	−0.0386	10.0
	$5_{51}-0_{00}$	305.38982	0.09484	10.0		$2_{12}-0_{00}$	37.7480	−0.0555	10.0
	$5_{50}-0_{00}$	305.95087	0.09887	10.0		$2_{11}-0_{00}$	50.5652	−0.0197	10.0
(0,2,0)[d]	0_{00}	2353.9655	0.1344	10.0		$2_{21}-0_{00}$	54.1754	−0.1199	10.0
	$1_{01}-0_{00}$	14.0496	0.0250	10.0		$2_{20}-0_{00}$	57.4394	−0.0896	10.0
	$1_{11}-0_{00}$	15.7203	0.0032	10.0		$3_{03}-0_{00}$	70.5287	−0.0857	10.0
	$1_{10}-0_{00}$	20.5557	0.0181	10.0		$3_{13}-0_{00}$	70.5526	−0.0888	10.0
	$2_{02}-0_{00}$	38.6065	0.0493	10.0		$3_{12}-0_{00}$	93.8767	−0.0728	10.0
	$2_{12}-0_{00}$	38.9864	0.0388	10.0		$3_{22}-0_{00}$	94.8348	−0.1440	10.0
	$2_{11}-0_{00}$	53.4736	0.0837	10.0		$3_{21}-0_{00}$	106.1697	−0.0489	10.0

TABLE I—*Continued*

(v_1, v_2, v_3)	$J'_{K'_a K'_c} - J''_{K''_a K''_c}$	obs.[a] cm^{-1}	o.–c. cm^{-1}	weight	(v_1, v_2, v_3)	$J'_{K'_a K'_c} - J''_{K''_a K''_c}$	obs.[a] cm^{-1}	o.–c. cm^{-1}	weight
(0,0,1)[d]	$3_{31} - 0_{00}$	113.2671	−0.2503	10.0	(0,1,1)[e]	$4_{41} - 0_{00}$	198.029	−0.400	1.0
	$3_{30} - 0_{00}$	115.4345	−0.2062	10.0		$4_{40} - 0_{00}$	199.293	−0.350	1.0
	$4_{04} - 0_{00}$	112.7576	−0.1403	10.0		$5_{05} - 0_{00}$	164.151	−0.076	1.0
	$4_{14} - 0_{00}$	112.7607	−0.1402	10.0		$5_{15} - 0_{00}$	164.156	−0.072	1.0
	$4_{13} - 0_{00}$	146.1660	−0.1600	10.0		$5_{14} - 0_{00}$	210.194	−0.084	1.0
	$4_{23} - 0_{00}$	146.3294	−0.1810	10.0		$5_{24} - 0_{00}$	210.225	−0.091	1.0
	$4_{22} - 0_{00}$	168.3089	−0.0990	10.0		$5_{23} - 0_{00}$	245.043	−0.036	1.0
	$4_{32} - 0_{00}$	171.0332	−0.2651	10.0		$5_{33} - 0_{00}$	245.895	−0.118	1.0
	$4_{31} - 0_{00}$	181.1490	−0.0658	10.0		$5_{32} - 0_{00}$	267.178	0.091	1.0
	$4_{41} - 0_{00}$	192.1241	−0.4277	10.0		$5_{42} - 0_{00}$	273.654	−0.254	1.0
	$4_{40} - 0_{00}$	193.3850	−0.3864	10.0		$5_{41} - 0_{00}$	280.345	−0.051	1.0
	$5_{05} - 0_{00}$	164.3095	−0.2055	10.0		$5_{51} - 0_{00}$	299.718	−0.621	1.0
	$5_{15} - 0_{00}$	164.3098	−0.2056	10.0		$5_{50} - 0_{00}$	300.370	−0.584	1.0
	$5_{14} - 0_{00}$	207.4048	−0.2453	10.0	(0,2,1)[f]	0_{00}	4939.23	−0.59	1.0
	$5_{24} - 0_{00}$	207.4270	−0.2501	10.0	(2,0,0)[f]	0_{00}	5145.12	−0.40	1.0
	$5_{23} - 0_{00}$	240.1296	−0.2299	10.0	(1,0,1)[f]	0_{00}	5147.36	0.24	1.0
	$5_{33} - 0_{00}$	240.7634	−0.3034	10.0	(2,1,0)[g]	0_{00}	6288.14277	−0.22421	10.0
	$5_{32} - 0_{00}$	260.8028	−0.1289	10.0		$1_{01} - 0_{00}$	13.51326	−0.02088	10.0
	$5_{42} - 0_{00}$	266.4658	−0.4201	10.0		$1_{11} - 0_{00}$	15.05217	0.05536	10.0
	$5_{41} - 0_{00}$	272.7071	−0.2764	10.0		$1_{10} - 0_{00}$	19.35556	−0.01191	10.0
	$5_{51} - 0_{00}$	290.7215	−0.6518	10.0		$2_{02} - 0_{00}$	37.23290	−0.04014	10.0
	$5_{50} - 0_{00}$	291.3866	−0.6217	10.0		$2_{12} - 0_{00}$	37.46697	0.00630	10.0
(1,1,0)[e]	0_{00}	3779.1710	−0.1165	10.0		$2_{11} - 0_{00}$	50.75556	−0.07256	10.0
	$1_{01} - 0_{00}$	13.692	−0.012	1.0		$2_{21} - 0_{00}$	55.13259	0.01412	10.0
	$1_{11} - 0_{00}$	15.158	0.021	1.0		$2_{20} - 0_{00}$	58.33656	−0.02930	10.0
	$1_{10} - 0_{00}$	19.653	0.002	1.0		$3_{03} - 0_{00}$	69.86905	−0.05489	10.0
	$2_{02} - 0_{00}$	37.729	−0.007	1.0		$3_{13} - 0_{00}$	69.69449	−0.04518	10.0
	$2_{12} - 0_{00}$	38.036	0.002	1.0		$3_{12} - 0_{00}$	94.12109	−0.11352	10.0
	$2_{11} - 0_{00}$	51.512	−0.034	1.0		$3_{22} - 0_{00}$	94.85002	0.19197	0.0
	$2_{21} - 0_{00}$	55.870	0.053	1.0		$3_{21} - 0_{00}$	106.76045	−0.14813	10.0
	$2_{20} - 0_{00}$	59.251	0.020	1.0		$3_{31} - 0_{00}$	115.40421	0.00907	10.0
	$3_{03} - 0_{00}$	70.621	0.002	1.0		$3_{30} - 0_{00}$	117.40283	−0.03656	10.0
	$3_{13} - 0_{00}$	70.664	0.003	1.0		$4_{04} - 0_{00}$	111.06701	−0.07781	10.0
	$3_{12} - 0_{00}$	95.471	−0.035	1.0		$4_{14} - 0_{00}$	111.06734	−0.07792	10.0
	$3_{22} - 0_{00}$	96.926	0.011	1.0		$4_{13} - 0_{00}$	146.24319	−0.14796	10.0
	$3_{21} - 0_{00}$	108.393	−0.063	1.0		$4_{23} - 0_{00}$	146.41318	−0.08029	10.0
	$3_{31} - 0_{00}$	116.736	0.067	1.0		$4_{22} - 0_{00}$	169.07466	−0.22957	10.0
	$3_{30} - 0_{00}$	119.272	0.066	1.0		$4_{32} - 0_{00}$	173.15648	−0.09910	10.0
	$4_{04} - 0_{00}$	112.575	0.008	1.0		$4_{31} - 0_{00}$	181.77319	−0.23829	10.0
	$4_{14} - 0_{00}$	112.578	0.005	1.0		$4_{41} - 0_{00}$	195.86148	0.01723	10.0
	$4_{13} - 0_{00}$	148.339	−0.013	1.0		$4_{40} - 0_{00}$	196.93597	−0.02189	10.0
	$4_{23} - 0_{00}$	148.641	0.004	1.0		$5_{05} - 0_{00}$	161.51201	−0.11118	10.0
	$4_{22} - 0_{00}$	171.593	−0.093	1.0		$5_{15} - 0_{00}$	161.51104	−0.11204	10.0
	$4_{32} - 0_{00}$	175.506	0.031	1.0		$5_{14} - 0_{00}$	206.91704	−0.17242	10.0
	$4_{31} - 0_{00}$	184.596	−0.086	1.0		$5_{24} - 0_{00}$	206.93537	−0.15816	10.0
	$4_{41} - 0_{00}$	199.228	0.139	1.0		$5_{23} - 0_{00}$	241.17477	−0.27838	10.0
	$4_{40} - 0_{00}$	200.088	0.145	1.0		$5_{33} - 0_{00}$	241.67051	−0.02959	10.0
	$5_{05} - 0_{00}$	163.693	0.020	1.0		$5_{32} - 0_{00}$	262.00045	−0.38507	10.0
	$5_{15} - 0_{00}$	163.694	0.020	1.0		$5_{42} - 0_{00}$	270.12168	−0.18546	10.0
	$5_{14} - 0_{00}$	209.898	0.009	1.0		$5_{41} - 0_{00}$	276.18989	−0.32675	10.0
	$5_{24} - 0_{00}$	209.948	0.012	1.0		$5_{51} - 0_{00}$	296.46957	0.03559	10.0
	$5_{23} - 0_{00}$	244.699	−0.058	1.0		$5_{50} - 0_{00}$	296.98654	0.00661	10.0
	$5_{33} - 0_{00}$	245.830	−0.001	1.0	(1,1,1)[g]	0_{00}	6289.17385	0.18142	10.0
	$5_{32} - 0_{00}$	265.979	−0.174	1.0		$1_{01} - 0_{00}$	13.39959	−0.07006	10.0
	$5_{42} - 0_{00}$	273.526	0.052	1.0		$1_{11} - 0_{00}$	14.91255	−0.00978	10.0
	$5_{41} - 0_{00}$	280.547	−0.088	1.0		$1_{10} - 0_{00}$	19.34693	−0.02068	10.0
	$5_{51} - 0_{00}$	301.302	0.283	1.0		$2_{02} - 0_{00}$	37.27361	−0.07490	10.0
	$5_{50} - 0_{00}$	301.745	0.266	1.0		$2_{12} - 0_{00}$	37.49371	−0.03559	10.0
(0,1,1)[e]	0_{00}	3789.272	−0.385	10.0		$2_{11} - 0_{00}$	50.70351	−0.08111	10.0
	$1_{01} - 0_{00}$	13.764	0.015	1.0		$2_{21} - 0_{00}$	55.00287	−0.04219	10.0
	$1_{11} - 0_{00}$	15.115	−0.028	1.0		$2_{20} - 0_{00}$	58.30436	−0.05506	10.0
	$1_{10} - 0_{00}$	19.635	−0.015	1.0		$3_{03} - 0_{00}$	69.70583	−0.08575	10.0
	$2_{02} - 0_{00}$	37.829	−0.008	1.0		$3_{13} - 0_{00}$	69.72859	−0.07722	10.0
	$2_{12} - 0_{00}$	38.084	−0.023	1.0		$3_{12} - 0_{00}$	94.77078	−0.37823	0.0
	$2_{11} - 0_{00}$	51.697	0.030	1.0		$3_{22} - 0_{00}$	95.44095	−0.10121	10.0
	$2_{21} - 0_{00}$	55.712	−0.108	1.0		$3_{21} - 0_{00}$	106.72522	−0.15079	10.0
	$2_{20} - 0_{00}$	59.138	−0.064	1.0		$3_{31} - 0_{00}$	115.22311	−0.08131	10.0
	$3_{03} - 0_{00}$	70.792	−0.030	1.0		$3_{30} - 0_{00}$	117.31007	−0.09977	10.0
	$3_{13} - 0_{00}$	70.827	−0.031	1.0		$4_{04} - 0_{00}$	111.13338	−0.12697	10.0
	$3_{12} - 0_{00}$	95.677	0.007	1.0		$4_{14} - 0_{00}$	111.13495	−0.12560	10.0
	$3_{22} - 0_{00}$	96.886	−0.069	1.0		$4_{13} - 0_{00}$	146.31450	−0.20742	10.0
	$3_{21} - 0_{00}$	108.999	0.075	1.0		$4_{23} - 0_{00}$	146.46427	−0.14997	10.0
	$3_{31} - 0_{00}$	116.682	−0.226	1.0		$4_{22} - 0_{00}$	168.91477	−0.24694	10.0
	$3_{30} - 0_{00}$	118.914	−0.165	1.0		$4_{32} - 0_{00}$	172.85030	−0.18987	10.0
	$4_{04} - 0_{00}$	112.870	−0.054	1.0		$4_{31} - 0_{00}$	181.73833	−0.24307	10.0
	$4_{13} - 0_{00}$	148.544	−0.047	1.0		$4_{41} - 0_{00}$	195.59795	−0.12726	10.0
	$4_{23} - 0_{00}$	148.765	−0.072	1.0		$4_{40} - 0_{00}$	196.74319	−0.14270	10.0
	$4_{22} - 0_{00}$	172.063	0.042	1.0		$5_{05} - 0_{00}$	161.62016	−0.18105	10.0
	$4_{32} - 0_{00}$	175.374	−0.145	1.0		$5_{15} - 0_{00}$	161.62081	−0.18025	10.0
	$4_{31} - 0_{00}$	184.429	0.056	1.0		$5_{14} - 0_{00}$	206.97828	−0.23600	10.0

TABLE I—*Continued*

(v_1,v_2,v_3)	$J'_{K'_a\,K'_c}-J''_{K''_a\,K''_c}$	obs.[a] cm^{-1}	o.−c. cm^{-1}	weight	(v_1,v_2,v_3)	$J'_{K'_a\,K'_c}-J''_{K''_a\,K''_c}$	obs.[a] cm^{-1}	o.−c. cm^{-1}	weight
(1,1,1)[g]	$5_{24}-0_{00}$	206.99278	−0.22350	10.0	(3,0,0)[f]	0_{00}	7576.3	−0.2	1.0
	$5_{23}-0_{00}$	241.67698	−0.47937	10.0	(2,0,1)[f]	0_{00}	7576.3	−0.1	1.0
	$5_{33}-0_{00}$	242.10667	−0.26081	10.0	(1,0,2)[f]	0_{00}	7751.9	−0.5	1.0
	$5_{32}-0_{00}$	261.92222	−0.36526	10.0	(0,0,3)[f]	0_{00}	7779.2	−0.4	1.0
	$5_{42}-0_{00}$	269.78961	−0.29257	10.0	(2,1,1)[f]	0_{00}	8697.3	0.8	1.0
	$5_{41}-0_{00}$	276.12066	−0.34872	10.0	(3,0,1)[f]	0_{00}	9911.05	0.30	1.0
	$5_{51}-0_{00}$	296.10542	−0.16993	10.0	(2,0,2)[f]	0_{00}	10188.25	−0.61	1.0
	$5_{50}-0_{00}$	296.67003	−0.18298	10.0	(1,0,3)[f]	0_{00}	10194.48	1.04	1.0
(0,1,2)[h]	0_{00}	6388.7306	2.8411	0.0	(3,1,1)[f]	0_{00}	11008.78	1.04	1.0
$D_2{}^{32}S$									
(0,0,0)[i]	0_{00}	0.0			(0,1,0)[j]	$5_{51}-0_{00}$	159.38024	0.09337	10.0
	$1_{01}-0_{00}$	6.95615	0.00193	100.0		$5_{50}-0_{00}$	159.50965	0.09380	10.0
	$1_{11}-0_{00}$	7.93561	0.00282	100.0	(1,0,0)[j]	0_{00}	1896.43169	0.58355	10.0
	$1_{10}-0_{00}$	10.00356	0.00327	100.0		$1_{01}-0_{00}$	6.88073	−0.00729	10.0
	$2_{02}-0_{00}$	19.50303	0.00583	100.0		$1_{11}-0_{00}$	7.85098	−0.00010	10.0
	$2_{12}-0_{00}$	19.78010	0.00622	100.0		$1_{10}-0_{00}$	9.90033	−0.00208	10.0
	$2_{11}-0_{00}$	25.98049	0.00751	100.0		$2_{02}-0_{00}$	19.28957	−0.01607	10.0
	$2_{21}-0_{00}$	28.91573	0.01033	100.0		$2_{12}-0_{00}$	19.56214	−0.01346	10.0
	$2_{20}-0_{00}$	30.27730	0.01021	100.0		$2_{11}-0_{00}$	25.70554	−0.02032	10.0
	$3_{03}-0_{00}$	36.79272	0.01127	100.0		$2_{21}-0_{00}$	28.61247	0.00104	10.0
	$3_{13}-0_{00}$	36.84521	0.01136	100.0		$2_{20}-0_{00}$	29.95103	−0.01226	10.0
	$3_{12}-0_{00}$	48.51662	0.01422	100.0		$3_{03}-0_{00}$	36.38505	−0.02967	10.0
	$3_{22}-0_{00}$	49.78228	0.01603	100.0		$3_{13}-0_{00}$	36.43582	−0.02938	10.0
	$3_{21}-0_{00}$	54.70730	0.01600	100.0		$3_{12}-0_{00}$	48.00092	−0.03614	10.0
	$3_{31}-0_{00}$	60.51585	0.02202	100.0		$3_{22}-0_{00}$	49.24599	−0.02533	10.0
	$3_{30}-0_{00}$	61.23489	0.02156	100.0		$3_{21}-0_{00}$	54.14869	−0.02630	10.0
	$4_{04}-0_{00}$	58.87438	0.01812	100.0		$3_{31}-0_{00}$	59.87758	0.00092	10.0
	$4_{14}-0_{00}$	58.88283	0.01813	100.0		$3_{30}-0_{00}$	60.51607	−0.05856	10.0
	$4_{13}-0_{00}$	76.05674	0.02319	100.0		$4_{04}-0_{00}$	58.21723	−0.04899	10.0
	$4_{23}-0_{00}$	76.40554	0.02389	100.0		$4_{14}-0_{00}$	58.22507	−0.04914	10.0
	$4_{22}-0_{00}$	86.71597	0.02456	100.0		$4_{13}-0_{00}$	75.24052	−0.05083	10.0
	$4_{32}-0_{00}$	89.97686	0.02937	100.0		$4_{23}-0_{00}$	75.57790	−0.04911	10.0
	$4_{31}-0_{00}$	93.43084	0.02790	100.0		$4_{22}-0_{00}$	85.80521	−0.06294	10.0
	$4_{41}-0_{00}$	102.82961	0.03842	100.0		$4_{32}-0_{00}$	89.00772	−0.04227	10.0
	$4_{40}-0_{00}$	103.14890	0.03795	100.0		$4_{31}-0_{00}$	92.55287	0.00800	10.0
	$5_{05}-0_{00}$	85.81837	0.02647	100.0		$4_{40}-0_{00}$	101.58440	−0.33981	10.0
	$5_{15}-0_{00}$	85.81964	0.02647	100.0		$5_{15}-0_{00}$	84.85678	−0.07383	10.0
	$5_{14}-0_{00}$	108.17297	0.03362	100.0		$5_{14}-0_{00}$	107.00010	−0.07319	10.0
	$5_{24}-0_{00}$	108.24640	0.03379	100.0		$5_{24}-0_{00}$	107.06932	−0.07346	10.0
	$5_{23}-0_{00}$	124.55923	0.03646	100.0		$5_{23}-0_{00}$	123.24326	−0.08196	10.0
	$5_{33}-0_{00}$	125.81526	0.03923	100.0		$5_{33}-0_{00}$	124.45944	−0.07625	10.0
	$5_{32}-0_{00}$	134.23405	0.03703	100.0		$5_{32}-0_{00}$	132.84279	−0.08602	10.0
	$5_{42}-0_{00}$	140.50879	0.04665	100.0		$5_{42}-0_{00}$	138.96525	−0.07880	10.0
	$5_{41}-0_{00}$	142.58619	0.04420	100.0		$5_{41}-0_{00}$	141.39235	0.10800	10.0
	$5_{51}-0_{00}$	155.91156	0.06020	100.0		$5_{51}-0_{00}$	153.57053	−0.45624	10.0
	$5_{50}-0_{00}$	156.03856	0.05986	100.0		$5_{50}-0_{00}$	154.96903	0.26828	10.0
(0,1,0)[j]	0_{00}	855.40420	−0.01381	10.0	(0,0,1)[j]	0_{00}	1910.18406	0.05830	10.0
	$1_{01}-0_{00}$	7.00738	0.00578	10.0		$1_{01}-0_{00}$	6.91453	0.00573	10.0
	$1_{11}-0_{00}$	8.04622	0.00470	10.0		$1_{11}-0_{00}$	7.83209	−0.01223	10.0
	$1_{10}-0_{00}$	10.21074	0.00694	10.0		$1_{10}-0_{00}$	9.89155	−0.00720	10.0
	$2_{02}-0_{00}$	19.59966	0.01480	10.0		$2_{02}-0_{00}$	19.35224	0.00194	10.0
	$2_{12}-0_{00}$	19.89668	0.01400	10.0		$2_{12}-0_{00}$	19.61411	0.00265	10.0
	$2_{11}-0_{00}$	26.38640	0.02069	10.0		$2_{11}-0_{00}$	25.77928	0.01078	10.0
	$2_{21}-0_{00}$	29.49916	0.01772	10.0		$2_{21}-0_{00}$	28.52850	−0.04308	10.0
	$2_{20}-0_{00}$	30.91729	0.02009	10.0		$2_{20}-0_{00}$	29.91417	−0.02932	10.0
	$3_{03}-0_{00}$	36.88411	0.02711	10.0		$3_{03}-0_{00}$	36.49032	−0.00651	10.0
	$3_{13}-0_{00}$	36.94111	0.02685	10.0		$3_{13}-0_{00}$	36.51978	−0.01811	10.0
	$3_{12}-0_{00}$	49.16533	0.03821	10.0		$3_{12}-0_{00}$	48.12710	0.01040	10.0
	$3_{22}-0_{00}$	50.51957	0.03498	10.0		$3_{22}-0_{00}$	49.35523	0.03414	10.0
	$3_{21}-0_{00}$	55.65837	0.04205	10.0		$3_{21}-0_{00}$	54.25598	0.01933	10.0
	$3_{31}-0_{00}$	61.81528	0.03676	10.0		$3_{31}-0_{00}$	59.69166	−0.09141	10.0
	$3_{30}-0_{00}$	62.55900	0.03865	10.0		$3_{30}-0_{00}$	60.44694	−0.07578	10.0
	$4_{04}-0_{00}$	58.90940	0.04332	10.0		$4_{04}-0_{00}$	58.39641	−0.01113	10.0
	$4_{14}-0_{00}$	58.91874	0.04329	10.0		$4_{14}-0_{00}$	58.40123	−0.01297	10.0
	$4_{13}-0_{00}$	76.92092	0.05810	10.0		$4_{13}-0_{00}$	75.38351	−0.01399	10.0
	$4_{23}-0_{00}$	77.29888	0.05638	10.0		$4_{23}-0_{00}$	75.58043	−0.08851	10.0
	$4_{22}-0_{00}$	88.07176	0.06853	10.0		$4_{22}-0_{00}$	86.03891	0.03385	10.0
	$4_{32}-0_{00}$	91.55293	0.06174	10.0		$4_{32}-0_{00}$	89.50290	0.29959	10.0
	$4_{31}-0_{00}$	95.13824	0.06845	10.0		$4_{31}-0_{00}$	92.65316	0.05513	10.0
	$4_{41}-0_{00}$	105.09138	0.06196	10.0		$4_{41}-0_{00}$	101.40760	−0.15856	10.0
	$4_{40}-0_{00}$	105.41900	0.06288	10.0		$5_{15}-0_{00}$	85.13483	−0.01482	10.0
	$5_{15}-0_{00}$	85.75150	0.06320	10.0		$5_{14}-0_{00}$	107.19556	−0.03441	10.0
	$5_{14}-0_{00}$	109.19171	0.08228	10.0		$5_{24}-0_{00}$	107.23775	−0.05018	10.0
	$5_{24}-0_{00}$	109.27234	0.08166	10.0		$5_{23}-0_{00}$	123.49125	0.00084	10.0
	$5_{23}-0_{00}$	126.34371	0.09676	10.0		$5_{33}-0_{00}$	124.26807	−0.22407	10.0
	$5_{33}-0_{00}$	127.70090	0.09151	10.0		$5_{32}-0_{00}$	133.21451	0.08010	10.0
	$5_{32}-0_{00}$	136.46498	0.10377	10.0		$5_{41}-0_{00}$	141.89126	0.46137	10.0
	$5_{42}-0_{00}$	143.14903	0.09352	10.0		$5_{51}-0_{00}$	153.72753	−0.24454	10.0
	$5_{41}-0_{00}$	145.28957	0.09867	10.0		$5_{50}-0_{00}$	153.87115	−0.23796	10.0

TABLE I—*Continued*

(v_1, v_2, v_3)	$J'_{K'_a K'_c} - J''_{K''_a K''_c}$	obs.[a] cm^{-1}	o.−c. cm^{-1}	weight	(v_1, v_2, v_3)	$J'_{K'_a K'_c} - J''_{K''_a K''_c}$	obs.[a] cm^{-1}	o.−c. cm^{-1}	weight
(1,1,0)[k]	0_{00}	2742.77	0.43	1.0					
(0,1,1)[k]	0_{00}	2754.44	−0.27	1.0					
(1,1,1)[l]	0_{00}	4592.32	0.59	1.0					
$HD^{32}S$									
(0,0,0)[i]	0_{00}	0.0			(0,1,0)[m]	0_{00}	1032.71523	0.04975	10.0
	$1_{01}-0_{00}$	8.15749	0.00294	100.0		$1_{01}-0_{00}$	8.21548	0.00877	10.0
	$1_{11}-0_{00}$	12.97701	0.00021	100.0		$1_{11}-0_{00}$	13.21798	0.00464	10.0
	$1_{10}-0_{00}$	14.68063	0.00173	100.0		$2_{02}-0_{00}$	24.22830	0.02412	10.0
	$2_{02}-0_{00}$	24.09399	0.00801	100.0		$2_{12}-0_{00}$	27.81310	0.01800	10.0
	$2_{12}-0_{00}$	27.58315	0.00461	100.0		$2_{11}-0_{00}$	33.30094	0.03002	10.0
	$2_{11}-0_{00}$	32.69265	0.00911	100.0		$2_{21}-0_{00}$	48.30055	0.01771	10.0
	$2_{21}-0_{00}$	47.14494	0.00097	100.0		$2_{20}-0_{00}$	48.71612	0.01954	10.0
	$2_{20}-0_{00}$	47.52133	0.00172	100.0		$3_{03}-0_{00}$	47.32739	0.04361	10.0
	$3_{03}-0_{00}$	47.15990	0.01409	100.0		$3_{13}-0_{00}$	49.46908	0.03748	10.0
	$3_{13}-0_{00}$	49.27676	0.01078	100.0		$3_{12}-0_{00}$	60.37908	0.06041	10.0
	$3_{12}-0_{00}$	59.43847	0.01945	100.0		$3_{22}-0_{00}$	72.91236	0.04472	10.0
	$3_{22}-0_{00}$	71.58622	0.00998	100.0		$3_{21}-0_{00}$	74.86534	0.05229	10.0
	$3_{21}-0_{00}$	73.36081	0.01321	100.0		$3_{31}-0_{00}$	102.69909	0.03384	10.0
	$3_{31}-0_{00}$	100.12980	0.00043	100.0		$3_{30}-0_{00}$	102.75953	0.03418	10.0
	$3_{30}-0_{00}$	100.18304	0.00059	100.0		$4_{04}-0_{00}$	76.88416	0.06666	10.0
	$4_{04}-0_{00}$	76.76626	0.02089	100.0		$4_{14}-0_{00}$	77.97501	0.06215	10.0
	$4_{14}-0_{00}$	77.86451	0.01844	100.0		$4_{13}-0_{00}$	95.83709	0.09732	10.0
	$4_{13}-0_{00}$	94.51811	0.03172	100.0		$4_{23}-0_{00}$	105.39894	0.07922	10.0
	$4_{23}-0_{00}$	103.87581	0.02132	100.0		$4_{22}-0_{00}$	110.62580	0.09684	10.0
	$4_{22}-0_{00}$	108.64693	0.02886	100.0		$4_{32}-0_{00}$	136.13488	0.07345	10.0
	$4_{32}-0_{00}$	133.28383	0.01374	100.0		$4_{31}-0_{00}$	136.54550	0.07565	10.0
	$4_{31}-0_{00}$	133.64612	0.01475	100.0		$4_{41}-0_{00}$	176.88971	0.05230	10.0
	$4_{41}-0_{00}$	172.39006	−0.00126	100.0		$4_{40}-0_{00}$	176.89690	0.05235	10.0
	$4_{40}-0_{00}$	172.39623	−0.00124	100.0		$5_{05}-0_{00}$	112.64832	0.09425	10.0
	$5_{05}-0_{00}$	112.66393	0.02890	100.0		$5_{15}-0_{00}$	113.14324	0.09168	10.0
	$5_{15}-0_{00}$	113.17190	0.02746	100.0		$5_{14}-0_{00}$	138.98943	0.13839	10.0
	$5_{14}-0_{00}$	137.31294	0.04467	100.0		$5_{24}-0_{00}$	145.49340	0.12064	10.0
	$5_{24}-0_{00}$	143.77034	0.03454	100.0		$5_{23}-0_{00}$	155.92872	0.15009	10.0
	$5_{23}-0_{00}$	153.34100	0.04732	100.0		$5_{33}-0_{00}$	177.98697	0.12204	10.0
	$5_{33}-0_{00}$	174.78359	0.02997	100.0		$5_{32}-0_{00}$	179.52854	0.12944	10.0
	$5_{32}-0_{00}$	176.14884	0.03342	100.0		$5_{42}-0_{00}$	218.64840	0.10401	10.0
	$5_{42}-0_{00}$	213.79797	0.01593	100.0		$5_{41}-0_{00}$	218.71195	0.10433	10.0
	$5_{41}-0_{00}$	213.85257	0.01612	100.0		$5_{51}-0_{00}$	270.91963	0.07222	10.0
	$5_{51}-0_{00}$	263.97724	−0.00398	100.0		$5_{50}-0_{00}$	270.92033	0.07216	10.0
	$5_{50}-0_{00}$	263.97788	−0.00398	100.0					
$H_2{}^{34}S$									
(0,1,0)[n]	0_{00}	1181.49820	0.15817	1.0	(2,1,0)[g]	0_{00}	6283.01238	−0.24514	1.0
(0,2,0)[d]	0_{00}	2351.83858	0.18222	1.0	(1,1,1)[g]	0_{00}	6283.95722	0.15636	1.0
(1,0,0)[d]	0_{00}	2612.36292	−0.30891	1.0	(0,1,2)[h]	0_{00}	6383.885	3.417	0.0
(0,0,1)[d]	0_{00}	2626.12100	−0.09682	1.0					

[a]Experimental energy spacings. Data labeled by (v_1, v_2, v_3) 0_{00} are vibrational term values measured relative to the (0,0,0) 0_{00} level of the isotopic molecule in question. Unless otherwise indicated, the other data are spacings within the particular (v_1, v_2, v_3) state. [b]Calculated from the rotation-vibration parameters of Ref. (*28*). [c]Vibrational energy from Ref. (*35*); rotational spacings calculated from the parameters of Ref. (*35*). [d]Ref. (*32*). [e]Vibrational energy from Ref. (*22*); Rotational spacings obtained by adding ground state term values to the experimental wavenumbers of Ref. (*22*). [f]Ref. (*15*). [g]Ref. (*36*). [h]Ref. (*36*). Uncertain observation (only a few perturbation induced transitions observed). Given zero weight in the fitting. [i]Calculated from the rotation-vibration parameters of Ref. (*34*). [j]Vibrational energy from Ref. (*37*); rotational spacings from Ref. (*28*). [k]Ref. (*16*). [l]Ref. (*14*). [m]Ref. (*28*). [n]Ref. (*35*).

also contains the force constant values obtained in a high-level ab initio calculation by Senekowitsch *et al.* (*41*) and those obtained by Kauppi and Halonen (*40*). For the second- and third-order force constants, there is clearly broad agreement between the three data sets in Table III, whereas the fourth-order ab initio constants show some discrepancy from the values obtained in the present work. In the calculation by Kauppi and Halonen (*40*), most fourth-order force constants were constrained to zero. The discrepancies between ab initio force constant values and MORBID values found here for H_2S are comparable to those obtained for H_2O (Table V of Ref. (*39*)) and H_2Se (Table III of Ref. (*9*)).

TABLE II

Fitted Potential Energy Parameters for H_2S

ρ_e/deg	87.77403(883)[a]		
r_{12}^e/Å	1.3365538(330)		
a_1/Å^{-1}	1.658530(927)		
$f_0^{(2)}$/cm^{-1}	19138.0(119)	$f_1^{(1)}$/cm^{-1}	−3280.3(873)
$f_0^{(3)}$/cm^{-1}	1414.5(650)	$f_1^{(2)}$/cm^{-1}	−6555.(149)
$f_0^{(4)}$/cm^{-1}	5337.4(626)	$f_{13}^{(0)}$/cm^{-1}	−333.89(633)
$f_{11}^{(0)}$/cm^{-1}	39198.8(389)	$f_{13}^{(2)}$/cm^{-1}	3660.(193)
$f_{11}^{(2)}$/cm^{-1}	−3151.(212)	$f_{111}^{(2)}$/cm^{-1}	−10049.(984)
$f_{113}^{(0)}$/cm^{-1}	−431.0(324)		

[a] Quantities in parentheses are standard errors in units of the last digit given.

Finally, we have used our fitted potential energy surface to calculate an extensive set of vibrational term values for $H_2{}^{32}S$, $D_2{}^{32}S$, and $HD^{32}S$. The results are given in Table IV. The basis sets were $N_{\text{Stretch}} = 12$, $N_{\text{Bend}} = 18$, and $(N_A, N_B) = (25, 20)$ for $H_2{}^{32}S$; $N_{\text{Stretch}} = 12$, $N_{\text{Bend}} = 20$, and $(N_A, N_B) = (30, 25)$ for $D_2{}^{32}S$; and $N_{\text{Stretch}} = 12$, $N_{\text{Bend}} = 22$, and $N_A = 55$ for $HD^{32}S$. The local mode behavior (*42, 43*) noted for $H_2{}^{80}Se$ in Refs. (*9, 10*) is also apparent for $H_2{}^{32}S$.

We have already pointed out that only rather few vibrational states of H_2S have been spectroscopically characterized. Clearly, Table I shows there to be even less data available for $D_2{}^{32}S$ and $HD^{32}S$. We hope that the predictions given in Table IV will encourage further experimental work on these molecules.

III. THE CALCULATION OF THE CLUSTER STATES

(a) Basis Set

We use the fitted potential energy function from Section II as input for a calculation of the cluster structure for $J \leqslant 40$ in the vibrational ground state and the ν_1, ν_2, ν_3, and $2\nu_2$ states of $H_2{}^{32}S$, again using the MORBID computer program (*11–13*). The calculation was done with a basis set defined by $N_{\text{Stretch}} = 7$, $N_{\text{Bend}} = 7$, and $(N_A, N_B) = (6, 4)$.

(b) Calculated Energies

The analysis given in the remainder of the present work is mainly concerned with the cluster formation in the vibrational ground state and the fundamental vibrational states of $H_2{}^{32}S$, and consequently we do not give lengthy tables of term values. As it was done for H_2Se (*9, 10*), the results are presented graphically in order to make the cluster structure apparent. However, all results from the calculation described here, as well as the results of calculations for other isotopic species of H_2S, are available from one of the authors (P.J.) on request.

The rotational energy level manifold in the vibrational ground state of $H_2{}^{32}S$ is shown in Fig. 2 for $J \leqslant 40$. The term values are plotted relative to the highest term

TABLE III

Equilibrium Geometry and Force Constants for H_2S

	ab initio[a]	KH[b]	This work
r_{12}^e/Å	1.3376	1.3356	1.3366
α_e[c]/deg	92.335	92.12	92.226
f_{rr}/aJ Å^{-2}	4.299	4.285	4.284
$f_{\alpha\alpha}$/aJ	0.765	0.763	0.759
$f_{rr'}$ /aJ Å^{-2}	−0.014	−0.020	−0.018
$f_{r\alpha}$/aJ Å^{-1}	0.076	0.121	0.108
f_{rrr}/aJ Å^{-3}	−22.5	−22.58	−21.314
$f_{\alpha\alpha\alpha}$/aJ	−0.28	−0.222	−0.257
$f_{rrr'}$/aJ Å^{-3}	−0.02	0.0	−0.048
$f_{rr\alpha}$/aJ Å^{-2}	−0.04	0.0	−0.179
$f_{rr'\alpha}$/aJ Å^{-2}	−0.19	−0.207	0.0
$f_{r\alpha\alpha}$/aJ Å^{-1}	−0.35	−0.267	−0.435
f_{rrrr}/aJ Å^{-4}	103.4	104.34	82.484
$f_{\alpha\alpha\alpha\alpha}$/aJ	−0.04	−0.770	−0.457
$f_{rrrr'}$/aJ Å^{-4}	−0.12		0.339
$f_{rrr'r'}$/aJ Å^{-4}	0.23		0.209
$f_{rrr\alpha}$/aJ Å^{-3}	−0.01		0.297
$f_{rrr'\alpha}$/aJ Å^{-3}	0.06		0.0
$f_{rr\alpha\alpha}$/aJ Å^{-2}	−0.46	−1.251	0.035
$f_{rr'\alpha\alpha}$/aJ Å^{-2}	0.49		0.399
$f_{r\alpha\alpha\alpha}$/aJ Å^{-1}	0.53		−0.058

[a]From Ref. (*41*). [b]From Ref. (*40*). [c]Equilibrium bond angle.

value for each J multiplet. The values calculated by the MORBID program (using the parameters from Table II) are given as horizontal lines, and experimentally derived term values are shown as circles. Filled circles represent term values that were included in the input data for the fitting ($J \leq 5$); empty circles represent term values that were not included.

Figure 2 shows the same qualitative pattern as that already found for the vibrational ground state of $H_2{}^{80}Se$ (see Fig. 2 of Ref. (*9*)). As J increases, the four highest energies in each J multiplet initially form two doublets, in agreement with the predictions from rigid rotor theory. However, from $J \approx 15$ the energy difference between the two doublets decreases with increasing J, and for high J values it tends toward zero so that fourfold clusters (referred to in Ref. (*10*) as Type I clusters) are formed. The so-called critical J value J_{CR}, at which the deviation from the customary rigid rotor picture becomes apparent (see Eq. (4) of Ref. (*1*)), is predicted by semiclassical theory as

$$J_{CR} = \frac{\omega}{4A} \sqrt{\frac{A - B}{C}}, \tag{8}$$

TABLE IV

Calculated Vibrational Levels

$H_2{}^{32}S$				$D_2{}^{32}S$				$HD^{32}S$			
v_1	v_2	v_3	/cm^{-1}	v_1	v_2	v_3	/cm^{-1}	v_1	v_2	v_3	/cm^{-1}
0	1	0	1182.44	0	1	0	855.42	0	1	0	1032.66
0	2	0	2353.83	0	2	0	1705.35	0	0	1	1902.71
1	0	0	2614.66	1	0	0	1895.85	0	2	0	2056.87
0	0	1	2628.56	0	0	1	1910.13	1	0	0	2621.89
0	3	0	3513.17	0	3	0	2549.40	0	1	1	2924.88
1	1	0	3779.29	1	1	0	2742.34	0	3	0	3071.97
0	1	1	3789.66	0	1	1	2754.71	1	1	0	3635.47
0	4	0	4659.48	0	4	0	3387.21	0	0	2	3756.02
1	2	0	4932.91	1	2	0	3583.36	0	2	1	3938.67
0	2	1	4939.82	0	2	1	3593.85	0	4	0	4077.30
2	0	0	5145.52	2	0	0	3752.80	1	0	1	4523.20
1	0	1	5147.12	1	0	1	3756.61	1	2	0	4640.64
0	0	2	5243.38	0	0	2	3808.79	0	1	2	4767.10
0	5	0	5791.83	0	5	0	4218.41	0	3	1	4943.40
1	3	0	6074.50	1	3	0	4418.52	0	5	0	5072.26
0	3	1	6078.05	0	3	1	4427.16	2	0	0	5147.97
2	1	0	6288.37	2	1	0	4588.87	1	1	1	5526.28
1	1	1	6288.99	1	1	1	4591.73	0	0	3	5559.95
0	1	2	6385.89	0	1	2	4643.56	1	3	0	5636.71
0	6	0	6909.29	0	6	0	5042.66	0	2	2	5769.88
1	4	0	7203.10	1	4	0	5247.45	0	4	1	5938.42
0	4	1	7203.39	0	4	1	5254.27	0	6	0	6056.25
1	2	1	7419.92	2	2	0	5419.40	2	1	0	6141.30
2	2	0	7420.03	1	2	1	5421.41	1	0	2	6375.04
0	2	2	7517.74	0	2	2	5473.03	1	2	1	6521.02
2	0	1	7576.42	3	0	0	5559.15	0	1	3	6559.34
3	0	0	7576.45	2	0	1	5559.57	1	4	0	6623.07
1	0	2	7752.40	1	0	2	5645.49	0	3	2	6763.68
0	0	3	7779.60	0	0	3	5672.74	0	5	1	6923.14
0	7	0	8010.95	0	7	0	5859.62	0	7	0	7028.66
0	5	1	8314.90	1	5	0	6069.79	2	0	1	7047.88
1	5	0	8317.74	0	5	1	6074.84	2	2	0	7126.26
1	3	1	8538.93	2	3	0	6243.99	0	0	4	7314.45
2	3	0	8539.53	1	3	1	6245.29	1	1	2	7367.00
0	3	2	8637.92	0	3	2	6296.81	1	3	1	7506.74
2	1	1	8696.48	3	1	0	6383.88	0	2	3	7550.55
3	1	0	8696.58	2	1	1	6384.12	3	0	0	7578.22
1	1	2	8877.73	1	1	2	6472.09	1	5	0	7599.09
0	1	3	8898.66	0	1	3	6496.01	0	4	2	7747.85
0	8	0	9095.86	0	8	0	6668.95	0	6	1	7896.93
0	6	1	9411.66	1	6	0	6885.17	0	8	0	7988.92
1	6	0	9417.50	0	6	1	6888.50	2	1	1	8030.76
1	4	1	9645.06	2	4	0	7062.28	2	3	0	8102.18
2	4	0	9645.95	1	4	1	7062.98	1	0	3	8177.36
0	4	2	9745.45	0	4	2	7114.53	0	1	4	8301.57
2	2	1	9805.37	3	2	0	7203.10	1	2	2	8350.72

TABLE IV—*Continued*

$H_2{}^{32}S$				$D_2{}^{32}S$				$HD^{32}S$			
v_1	v_2	v_3	/cm^{-1}	v_1	v_2	v_3	/cm^{-1}	v_1	v_2	v_3	/cm^{-1}
3	2	0	9805.50	2	2	1	7203.22	1	4	1	8482.80
3	0	1	9910.75	1	2	2	7293.35	0	3	3	8532.86
4	0	0	9910.77	0	2	3	7313.92	3	1	0	8550.18
1	2	2	9992.23	4	0	0	7314.47	1	6	0	8564.16
				3	0	1	7314.50	0	5	2	8721.77
				2	0	2	7452.42	0	7	1	8859.22
				1	0	3	7462.20	2	0	2	8898.33
				0	9	0	7470.32	0	9	0	8936.41
				0	0	4	7518.97	2	2	1	9005.35
				1	7	0	7693.26	0	0	5	9019.60
				0	7	1	7694.93	2	4	0	9068.43
				2	5	0	7873.90	1	1	3	9157.43
				1	5	1	7874.14	0	2	4	9280.65
				0	5	2	7925.83	1	3	2	9325.51
				3	3	0	8016.46	1	5	1	9448.58
				2	3	1	8016.49	3	0	1	9476.71
				1	3	2	8108.88	0	4	3	9505.62
				0	3	3	8126.12	3	2	0	9513.82
				4	1	0	8127.74	1	7	0	9517.71
				3	1	1	8127.75	0	6	2	9684.82
				0	10	0	8263.36	0	8	1	9809.41
				2	1	2	8268.70	2	1	2	9870.06
				1	1	3	8276.26	0	10	0	9870.52
				0	1	4	8331.87	4	0	0	9912.69
				1	8	0	8493.71	1	0	4	9929.81
				0	8	1	8493.78	2	3	1	9970.98
				1	6	1	8678.40	0	1	5	9994.33

where ω is the harmonic vibration wavenumber of the bending mode and A, B, and C are the rotational constants. Using the rotational constants from Ref. (*34*) and the bending fundamental energy from Ref. (*37*), we obtain $J_{CR} = 15$ for $H_2{}^{32}S$. Previously, Makarewicz (*6*) and Pyka (*7*) have obtained $J_{CR} = 16$ and 18, respectively. These results are in accordance with our observation from Fig. 2 that the energy distance between the two rigid rotor doublets at highest energy starts decreasing at $J = 15$. For $H_2{}^{80}Se$, the corresponding number is $J_{CR} = 12$ (*1*). For $H_2{}^{32}S$ at $J > 33$, the energy splitting between the two doublet components forming the cluster at highest energy is not visible on the scale of Fig. 2. This splitting is 0.26 cm^{-1} at $J = 34$ (where the two doublet components are calculated at 10 772.15 and 10 771.89 cm^{-1}, respectively, with the energy zero taken as the energy of the $J_{K_aK_c} = 0_{00}$ level of the vibrational ground state) and decreases to less than 0.001 cm^{-1} at $J = 40$, where the cluster components are calculated at 16 750.03 cm^{-1}. As J increases above 35, more fourfold clusters are formed in the J multiplets. At $J > 38$, the eight highest energies in each J multiplet form two fourfold clusters, and the energy difference between the two clusters increases linearly with J.

We may compare our calculated term values for the vibrational ground state of $H_2{}^{32}S$ at $J = 40$ with the results of Pyka (*7*) obtained in a rigid bender-type calculation

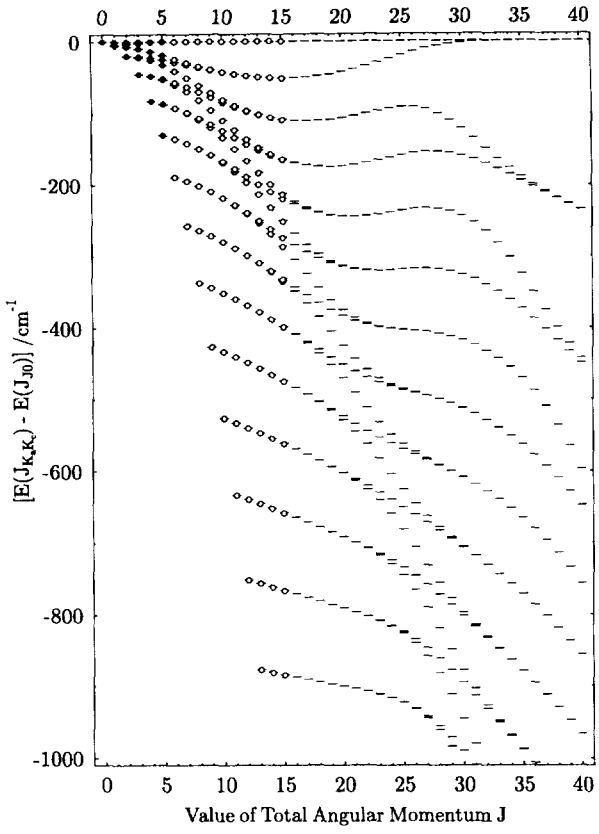

FIG. 2. The rotational energy level structure in the vibrational ground state of $H_2{}^{32}S$. Term values are plotted relative to the highest term value for each J multiplet. The term values calculated by the MORBID program (using the parameters from Table II) are given as horizontal lines, and experimental term values are shown as circles. Filled circles represent term values that were included in the input data for the MORBID fitting ($J \leq 5$); empty circles represent experimental term values that were not included.

neglecting the stretching motion. We determine the energies in the $J = 40$ multiplet to be systematically lower than those of Ref. (*7*), the difference increasing from approximately 100 cm^{-1} for the lowest energies of the multiplet to 1000 cm^{-1} for the highest energies. We attribute these deviations to the fact that we account explicitly for the stretching motion of H_2S. In Section IV we give estimates of the bond length displacements brought about by rotational excitation.

We do not give any results for the ν_2 state of $H_2{}^{32}S$ here. As already found for $H_2{}^{80}Se$ in Ref. (*10*), the cluster formation in this state is merely a repetition of that in the vibrational ground state.

Figure 3 is a term value diagram for $H_2{}^{32}S$ showing $\nu_1/\nu_3/2\nu_2$ energy levels with $J \leq 40$. The three energies present for $J = 0$ are the ν_3 (at 2628 cm^{-1}), ν_1 (at 2614 cm^{-1}), and $2\nu_2$ (at 2354 cm^{-1}) levels. We plot the energies relative to $E^{gs}(J_{J0})$ defined as the highest energy in each J multiplet of *vibrational ground state*. Careful comparison of Fig. 3 with Fig. 3 of Ref. (*10*) shows that the cluster formation in the ν_1/ν_3 interacting vibrational states of $H_2{}^{32}S$ follows exactly the same qualitative pattern as that described

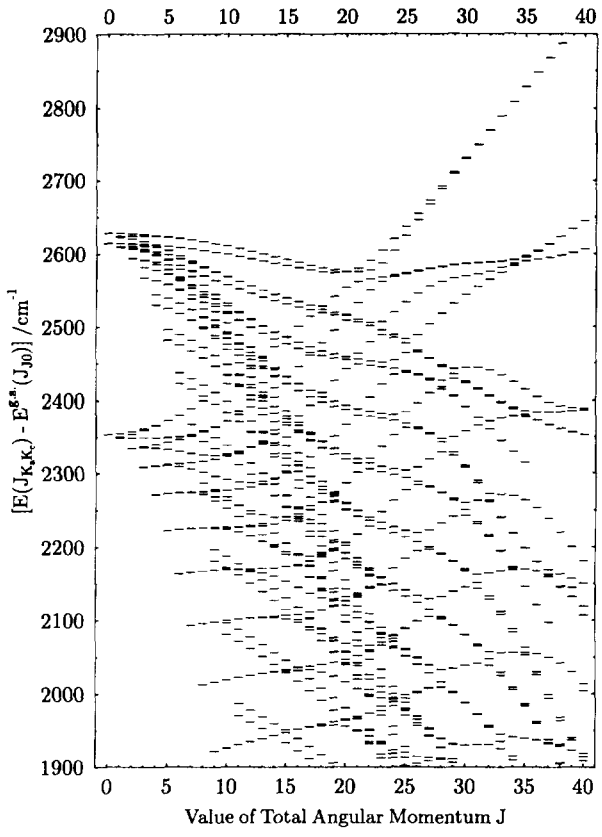

FIG. 3. An overview of the rotation-vibration term values calculated for $H_2{}^{32}S$ in the $\nu_1/\nu_3/2\nu_2$ region. The term values are plotted relative to the highest energy for each J multiplet *in the vibrational ground state*. The three states present for $J = 0$ are the ν_3 (at 2628 cm^{-1}), ν_1 (at 2614 cm^{-1}), and $2\nu_2$ (at 2354 cm^{-1}) levels.

in detail for $H_2{}^{80}Se$ in Ref. (*10*). For moderate J values, doublets of ν_1 or ν_3 rovibrational levels are formed as predicted by rigid rotor theory. However, when J increases, the ν_1 doublet at highest energy merges with the ν_3 doublet at highest energy to form a fourfold cluster (referred to in Ref. (*10*) as a Type II cluster), and when J increases further more clusters of this type are formed by the doublets at lower energies in the J multiplets. The details of this cluster formation can be seen for $H_2{}^{80}Se$ in Fig. 4a of Ref. (*10*). As already mentioned in Section I, Lehmann (*8*) discussed Type II clusters for the $v_1 + v_3 = 3$ vibrational states of $H_2{}^{80}Se$ prior to our quantum mechanical calculation of them (*10*). In the $2\nu_2$ state of $H_2{}^{32}S$, whose rovibrational levels are interlaced with the ν_1 and ν_3 levels, Type I clusters are in principle formed exactly as in the vibrational ground state. However, their pattern is often distorted by local interactions with ν_1 and ν_3. We note, for example, in Fig. 3 that the top cluster (the cluster at highest energy) in the ν_1/ν_3 state undergoes an avoided crossing with the top cluster in the $2\nu_2$ state at $J \approx 22$. At $J = 20$, the cluster at highest energy in Fig. 3 belongs to the ν_1/ν_3 state; the two doublets forming the cluster are calculated at 6618.48 and 6617.21 cm^{-1}, respectively, so they are split by 1.27 cm^{-1} which is barely

visible on the scale of the figure. The two highest $2\nu_2$ doublets are found at 6595.93 and 6559.51 cm^{-1}, respectively; they are split by 36.42 cm^{-1}. In the crossing region, for $J = 21$ through 25, the ν_1/ν_3 cluster is destroyed through interactions with the components of the two highest $2\nu_2$ doublets. Each of the four near-degenerate components in the ν_1/ν_3 cluster interacts with a partner state (of the same symmetry) in the two highest $2\nu_2$ doublets, and since these two doublets are still far from being degenerate, the interactions split the ν_1/ν_3 cluster components apart. After the avoided crossing at $J = 26$, the cluster at highest energy in Fig. 3 belongs to the $2\nu_2$ state; the two doublets forming the cluster are calculated at 9222.77 and 9214.21 cm^{-1}, respectively, and the splitting is 8.56 cm^{-1}. The doublet components of the highest ν_1/ν_3 cluster are found at 9145.15 and 9143.88 cm^{-1}, respectively, with a splitting of 1.27 cm^{-1}. For $H_2{}^{80}Se$ (Figs. 3 and 4a of Ref. (*10*)) the analogous avoided crossing takes place at around $J = 29$. At this J value, both the top cluster of the ν_1/ν_3 state and that of the $2\nu_2$ state are degenerate to within a fraction of a cm^{-1}, and the clusters are not destroyed by the avoided crossing. The interaction between the near-degenerate components of the ν_1/ν_3 cluster with their respective partner states in the $2\nu_2$ cluster displaces each component by the same amount of energy.

The ν_1/ν_3 cluster at highest energy experiences another less drastic avoided crossing with a partly formed $2\nu_2$ cluster around $J = 35$. Eventually at $J = 38$ (the last J value for which the top $2\nu_2$ cluster is visible on Fig. 3) the top ν_1/ν_3 cluster (calculated at 15 796.26 cm^{-1}) and the top $2\nu_2$ cluster (calculated at 16 085.76 cm^{-1}) are both degenerate to within 0.001 cm^{-1}.

IV. THE WAVEFUNCTION ANALYSIS

(a) Method

The ideas presented in the present section have been discussed previously at considerable length in Refs. (*9, 10*), and we only give a very brief summary here. We are concerned with rotation–vibration wavefunctions given as linear combinations of "primitive" basis functions $|n_1 n_3\rangle|v_2, |k|\rangle|J, k, M\rangle$:

$$\psi(r_1, r_3, \rho, \theta, \phi, \chi) = \sum_{n_1,n_3,v_2} \sum_{k=-J}^{J} c_{n_1,n_3,v_2,k} |n_1, n_3\rangle |v_2, |k|\rangle |J, k, M\rangle. \quad (9)$$

The wavefunction depends on the internuclear distances r_j, $j = 1$ or 3, defined in Section II, on the bending coordinate ρ defined in Ref. (*11*), and on the three Euler angles θ, ϕ, and χ describing the molecular rotation (*11*). The bending coordinate ρ is the bond angle supplement of the so-called *reference configuration* (see Ref. (*11*) and references therein) which follows the rotation and the bending motion of the molecule. The angle ρ is almost, but not quite, equal to the instantaneous value of the bond angle supplement $\bar{\rho}$ defined in Section II. In Eq. (9), $|J, k, M\rangle$ is an eigenfunction for a rigid symmetric top, the function $|v_2, |k|\rangle$ is a so-called rigid bender function obtained as an eigenfunction for the Hamiltonian $\hat{H}_{\text{Bend}}$ given in Eq. (63) of Ref. (*11*), and

$$|n_1 n_3\rangle = \Phi_{n_1}^{(1)}(r_1)\Phi_{n_3}^{(3)}(r_3) \quad (10)$$

is the product of two Morse oscillator eigenfunctions $\Phi_{n_j}^{(j)}(r_j)$, one for each internuclear distance (see Ref. (*11*)).

In the present work, we are concerned with wavefunctions given by Eq. (9). These functions can be MORBID eigenfunctions, in which case the expansion coefficients $c_{n_1,n_3,v_2,k}$ of Eq. (9) are obtained directly as eigenvector coefficients from the MORBID program or they are the functions referred to in Ref. (*10*) as *primitive cluster functions* or *primitive cluster states* (PCSs). The primitive cluster states are introduced as follows: We neglect the small energy splittings between the individual states in a fourfold cluster and consider the four cluster states to be exactly degenerate. In this case the cluster is represented by a four-dimensional space of degenerate eigenfunctions for the rotation–vibration Hamiltonian. One possible set of basis vectors in this space consists of the four eigenfunctions obtained directly in the MORBID calculation. Each of these four eigenfunctions transforms according to one of the irreducible representations A_1, A_2, B_1, and B_2 of the molecular symmetry group of H_2S, $C_{2v}(M)$ (*44*). We denote the MORBID eigenfunctions defining a cluster as $|i; A_1\rangle$, $|i; A_2\rangle$, $|i; B_1\rangle$, and $|i; B_2\rangle$, where i symbolizes suitable quantum numbers characterizing the cluster. We showed in Ref. (*9*) that there exists another possible choice of basis vectors in the four-dimensional space of degenerate eigenfunctions, the primitive cluster states $|\text{PCS}\,j\rangle, j = 1, 2, 3, 4$, suggested by semiclassical theory. These functions are obtained from the MORBID eigenfunctions through a unitary transformation (a rotation in the four-dimensional eigenfunction space),

$$|\text{PCS}\,j\rangle = c^{(j)}_{i;A_1}|i; A_1\rangle + c^{(j)}_{i;A_2}|i; A_2\rangle + c^{(j)}_{i;B_1}|i; B_1\rangle + c^{(j)}_{i;B_2}|i; B_2\rangle, \qquad (11)$$

where the expansion coefficients $c^{(j)}_{i;\Gamma}$ ($\Gamma = A_1, A_2, B_1, B_2; j = 1, 2, 3, 4$) are obtained from group theory (*3, 9, 10*). The functions $|\text{PCS}\,j\rangle$ are not symmetrized in $C_{2v}(M)$. As already discussed in Section I, two of the four primitive cluster functions will have angular momentum projections of $-\hbar J$ and $\hbar J$, respectively, along an axis A which lies approximately along one of the S–H bonds, and the other two functions will have angular momentum projections of $-\hbar J$ and $\hbar J$, respectively, along an axis A' which lies approximately along the other S–H bond (see Fig. 1). The primitive cluster wavefunctions can be expressed by Eq. (9) since they are linear combinations of MORBID eigenfunctions, each of which is a linear combination of the primitive basis functions. For a primitive cluster wavefunction $|\text{PCS}\,j\rangle$, the expansion coefficients $c_{n_1,n_3,v_2,k}$ of Eq. (9) are linear combinations of MORBID eigenvector coefficients.

In order to analyze the rotational and vibrational motion governed by the wavefunctions under study, we determine three quantities from these wavefunctions:

(1) the k probability p_k given by

$$p_k = \sum_{n_1,n_3,v_2} |c_{n_1,n_3,v_2,k}|^2 \qquad (12)$$

allows us to identify the localization axes A and A' (see Fig. 1). These axes are discussed extensively in Ref. (*9*). For a molecule, whose wavefunction is given by Eq. (9), p_k is the probability of finding the molecule with an angular momentum projection of $\hbar k$ on the molecule-fixed z axis (Fig. 1).

(2) the probability density in (r_1, r_3) space for the wavefunctions in Eq. (9), defined as

$$\mathcal{P}(r_1, r_3) = \int_0^{\pi} d\rho \int_0^{\pi} \sin\theta d\theta \int_0^{2\pi} d\phi \int_0^{2\pi} d\chi |\psi(r_1, r_3, \rho, \theta, \phi, \chi)|^2 \qquad (13)$$

so that the differential quantity

$$dP = \mathcal{P}(r_1, r_3)dr_1 dr_3 \tag{14}$$

is the probability of finding the molecule described by the wavefunction $\psi(r_1, r_3, \rho, \theta, \phi, \chi)$ in the volume element $dr_1 dr_3$ of (r_1, r_3) space.

(3) the quantum mechanical expectation values of the internuclear distances r_1 and r_3 (Fig. 1), obtained as

$$\overline{r_j} = \int_0^\infty dr_1 \int_0^\infty dr_3 r_j \mathcal{P}(r_1, r_3), \tag{15}$$

$j = 1$ or 3.

(b) k Probabilities

Following Refs. (*9, 10*), we have calculated the k probabilities p_k (Eq. (12)) for the primitive cluster states $|\text{PCS}\, j\rangle$ of H_2S. The function $|\text{PCS } 1\rangle$ is obtained as (see Eq. (11) and Eq. (3) of Ref. (*10*))

$$|\text{PCS } 1\rangle = \tfrac{1}{2}(|i; A_1\rangle + |i; A_2\rangle + |i; B_1\rangle + |i; B_2\rangle). \tag{16}$$

In Fig. 4, the k probabilities calculated for the function $|\text{PCS } 1\rangle$ in the top cluster of the vibrational ground state at $J = 20$, 30, and 40, respectively, are given as empty circles. The filled circles in Fig. 4 represent the k probabilities for the wavefunction $R_x^{(\varphi)}|\text{PCS } 1\rangle$ obtained by rotating $|\text{PCS } 1\rangle$ through an angle φ around the molecule-fixed x axis (the axis perpendicular to the molecular plane; see Fig. 1). We determine the angle φ so that the rotated function $R_x^{(\varphi)}|\text{PCS } 1\rangle$ has the "sharpest" possible k distribution, i.e.; by varying φ we aim at obtaining a rotated function $R_x^{(\varphi)}|\text{PCS } 1\rangle$ which, for one particular k value, k_{Local} say, has a k probability $p_{k_{\text{Local}}} \approx 1$, and k probabilities $p_k \approx 0$ for $k \neq k_{\text{Local}}$. In this way, we obtained $\varphi = 20°$ for $J = 20$, $\varphi = 32°$ for $J = 30$, and $\varphi = 38°$ for $J = 40$, where in all cases $k_{\text{Local}} = J$.

It is obvious from Fig. 4 that for the rotated function $R_x^{(\varphi)}|\text{PCS } 1\rangle$, $p_J \approx 1$, and $p_k \approx 0$ for $k < J$. Hence the rotated function has a defined angular momentum projection of $\hbar J$ on the molecule-fixed z axis so that the original function $|\text{PCS } 1\rangle$ must have a defined angular momentum projection of $\hbar J$ on the axis A defined in Fig. 1; this axis is close to the S–H_3 bond.

In the state $|\text{PCS } 1\rangle$, the total angular momentum has the largest possible projection on the A axis. Hence we can express the results of the rotational analysis described here in a less rigorous way by saying that the angular momentum is directed along the A axis, at least to the extent that quantum mechanics allows an angular momentum to have a defined direction. That is, the angular momentum is directed along the S–H_3 bond (Fig. 1). Classically one would now say that as the angular momentum is conserved in time, it has a constant direction in space and the molecule rotates around this direction. Consequently, our rotational analysis leads us to the conclusion that in the state $|\text{PCS } 1\rangle$, the molecule rotates around the S–H_3 bond.

A k-probability analysis for the primitive cluster state $|\text{PCS } 2\rangle$ (which can be obtained from Eq. (4) of Ref. (*10*)) shows that in this state, the molecule rotates around the S–H_1 bond. The primitive cluster states $|\text{PCS } 3\rangle$ and $|\text{PCS } 4\rangle$ can be obtained by letting the spatial inversion operation E^* (*44*) act on the functions $|\text{PCS } 1\rangle$ and $|\text{PCS } 2\rangle$. It can be straightforwardly shown that in the state $|\text{PCS } 3\rangle$, the

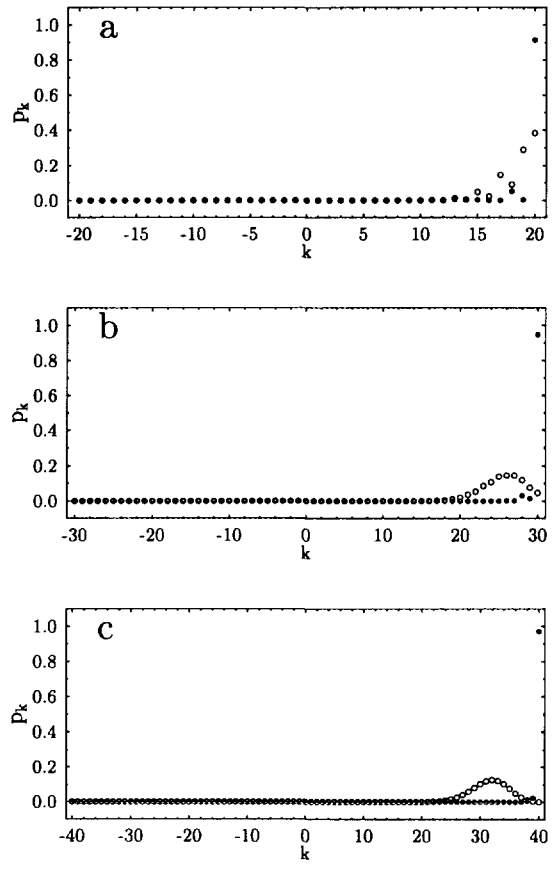

FIG. 4. The k distributions of localized rotational states in the vibrational ground state of $H_2{}^{32}S$. The figures show one state in the cluster at highest energy for (a) $J = 20$, (b) $J = 30$, and (c) $J = 40$, respectively. The empty circles show the k probabilities p_k for the localized wavefunction $|\text{PCS } 1\rangle$ and the filled circles show the analogous k probabilities for the function $R_x^{(\varphi)}|\text{PCS } 1\rangle$ obtained by rotating $|\text{PCS } 1\rangle$ through an angle φ around the molecule-fixed x axis (the axis perpendicular to the molecular plane; see Fig. 1).

molecule rotates around the S–H_3 bond, and in the state $|\text{PCS } 4\rangle$ it rotates around the S–H_1 bond.

We have already pointed out that the formation of Type I clusters in the ν_2 vibrational state of $H_2{}^{32}S$ is a repetition of that in the vibrational ground state. Consequently, a k-probability analysis of the primitive cluster wavefunctions found in the ν_2 state yields basically the same results as those described here for the vibrational ground state. In Ref. (*10*) we showed that for the primitive cluster states of $H_2{}^{80}Se$ corresponding to the Type II clusters at highest energy in the ν_1/ν_3 vibrational state, the rotational motion could be interpreted as a rotation around one of the bonds, exactly as found for Type I clusters. We do not give here the results of the Type II analysis for $H_2{}^{32}S$. It leads to k-probability plots indistinguishable from Fig. 4.

(c) Probability Density Functions

In Refs. (*9, 10*) we studied the probability density functions $\mathcal{P}(r_1, r_3)$ (Eq. (13)) for a number of rotation–vibration wavefunctions of $H_2{}^{80}Se$, including

(1) noncluster wavefunctions such as those representing the $J = 0$ levels in the vibrational ground state and in the ν_1 and ν_3 vibrational states,

(2) Type I cluster wavefunctions such as the primitive cluster function $|\text{PCS } 1\rangle$ for the cluster at highest energy at $J = 20$ in the vibrational ground state, and

(3) Type II cluster wavefunctions such as the primitive cluster functions $|\text{PCS } 1\rangle$ and $|\text{PCS } 2\rangle$ for the cluster at highest energy in the ν_1/ν_3 vibrational state at $J = 20$ and 30, respectively.

We concluded that the noncluster wavefunctions and the Type I cluster wavefunctions produced probability density functions very similar to those predicted by harmonic oscillator theory. For example, in the vibrational ground state both the noncluster function at $J = 0$ and the primitive cluster function $|\text{PCS } 1\rangle$ at $J = 20$ yield probability density functions which are well approximated by a two-dimensional Gaussian (Fig. 6 of Ref. (*10*)). The noncluster wavefunction obtained for $J = 0$ in the ν_1 vibrational state gives a probability density function which would be well approximated by that obtained from a wavefunction given as a product of two harmonic oscillator functions, one having $v_1 = 1$ and depending on a normal coordinate Q_1 proportional to $(r_1 - r_1^e) + (r_3 - r_3^e)$ and the other having $v_3 = 0$ and depending on a normal coordinate Q_3 proportional to $(r_1 - r_1^e) - (r_3 - r_3^e)$ (Fig. 7a of Ref. (*10*)). Similarly, the noncluster wavefunction obtained for $J = 0$ in the ν_3 vibrational state has a probability density function which would be well approximated by that obtained from an analogous product, in which the harmonic oscillator function depending on Q_1 has $v_1 = 0$ and that depending on Q_3 has $v_3 = 1$ (Fig. 7b of Ref. (*10*)).

The Type II cluster wavefunctions obtained from the MORBID program produce probability density functions very different from those predicted by harmonic oscillator theory. For the MORBID eigenfunctions belonging to the top cluster in the ν_1/ν_3 vibrational state at $J = 20$, the probability density functions are "volcano"-shaped for $H_2{}^{80}Se$ (Fig. 9 of Ref. (*10*)). At the equilibrium geometry the probability density is very small, but this point is surrounded by a "rampart" of probability. However, if we rotate the symmetrized MORBID eigenfunctions into the primitive cluster states $|\text{PCS } j\rangle$ for this cluster, we obtain very simple probability density functions (Fig. 10 of Ref. (*10*)). These functions now have local mode character in that the stretching excitation is localized in one bond, and the other bond oscillator is in its ground state. From the rotational analysis of the primitive cluster states $|\text{PCS } j\rangle$ in the top clusters of the ν_1/ν_3 vibrational state, we know that in these states, the molecule rotates around one of its bonds. The vibrational analysis outlined here shows that simultaneously, the stretching vibrational excitation is localized in one bond. This bond is in fact the one around which the molecule rotates. The other bond oscillator, which is in its ground state, is approximately perpendicular to the rotation axis and lengthens with increasing J due to centrifugal distortion (*10*).

For the noncluster wavefunctions and the Type I cluster functions of $H_2{}^{32}S$, the probability density functions are essentially repetitions of the corresponding functions for $H_2{}^{80}Se$ given in Ref. (*10*), and we do not report them here. For the top clusters in the ν_1/ν_3 vibrational state, there is some difference in detail between $H_2{}^{32}S$ and $H_2{}^{80}Se$, and we give here a few results for $H_2{}^{32}S$.

Figure 5 shows the probability density functions $\mathcal{P}(r_1, r_3)$ from Eq. (13) for (a) the MORBID eigenfunction with symmetry A_1, and (b) the MORBID eigenfunction with symmetry A_2 belonging to the top cluster in the ν_1/ν_3 state at $J = 20$ for $H_2{}^{32}S$.

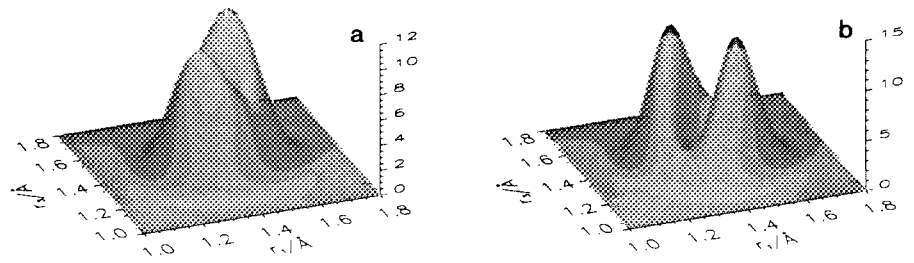

FIG. 5. Probability density ($Å^{-2}$) functions $\mathcal{P}(r_1, r_3)$ from Eq. (13) for (a) the MORBID eigenfunction with symmetry A_1 and (b) the MORBID eigenfunction with symmetry A_2 belonging to the cluster at highest energy in the ν_1/ν_3 state at $J = 20$ for $H_2{}^{32}S$.

This figure should be compared with Fig. 9 of Ref. (*10*), which is the analogous figure for $H_2{}^{80}Se$. The volcano shape found for $H_2{}^{80}Se$ is not so pronounced for $H_2{}^{32}S$. Obviously the mixing between the ν_1 and the ν_3 basis states is less for $H_2{}^{32}S$, since the A_1 function is clearly predominantly a ν_1 vibrational function, and the A_2 function is predominantly a ν_3 vibrational function (cf. Fig. 7 of Ref. (*10*)). Further, it should be noted that as described above, in $H_2{}^{32}S$ an avoided crossing of the cluster considered here with the top cluster of the $2\nu_2$ vibrational states takes place at $J \approx 22$. Hence at $J = 20$ there is already some mixing with the $2\nu_2$ basis states leading to a distortion of the probability density function.

In Fig. 6 we show the probability density functions $\mathcal{P}(r_1, r_3)$ from Eq. (13) for (a) the first primitive cluster state $|\text{PCS } 1\rangle$, and (b) the second primitive cluster state $|\text{PCS } 2\rangle$ belonging to the cluster at highest energy in the ν_1/ν_3 state at $J = 20$ for $H_2{}^{32}S$. This figure is almost indistinguishable from Fig. 10 of Ref. (*10*) (apart from the fact that the probability density functions are somewhat displaced in the (r_1, r_3) plane to account for the difference in equilibrium bond length between H_2S and H_2Se). We see that the stretching excitation is localized in the $S\text{–}H_3$ bond for $|\text{PCS } 1\rangle$ and in the $S\text{–}H_1$ bond for $|\text{PCS } 2\rangle$.

In order to show that the probability density function for a Type II cluster state is significantly different from that of a noncluster state, we given in Fig. 7 the $H_2{}^{32}S$ probability density functions $\mathcal{P}(r_1, r_3)$ for (a) the ν_1 state of lowest energy in the $J = 20$ manifold, $J_{K_aK_c} = 20_{0\,20}$, and (b) the ν_3 state of lowest energy for $J = 20$, $J_{K_aK_c} = 20_{0\,20}$. These functions are indistinguishable from the $\mathcal{P}(r_1, r_3)$ functions for the $J = 0$ levels of the ν_1 and ν_3 states, respectively (see Fig. 7 of Ref. (*10*)).

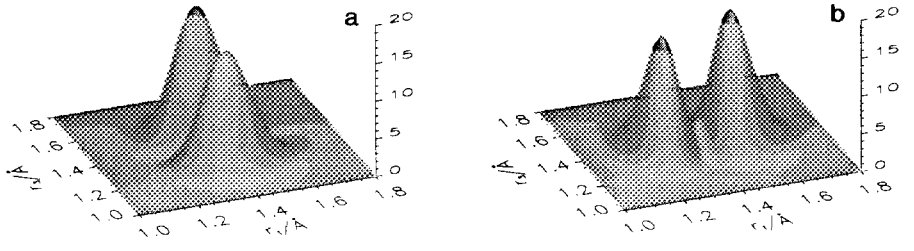

FIG. 6. Probability density ($Å^{-2}$) functions $\mathcal{P}(r_1, r_3)$ from Eq. (13) for (a) the first primitive cluster state $|\text{PCS } 1\rangle$ and (b) the second primitive cluster state $|\text{PCS } 2\rangle$ belonging to the cluster at highest energy in the ν_1/ν_3 state at $J = 20$ for $H_2{}^{32}S$.

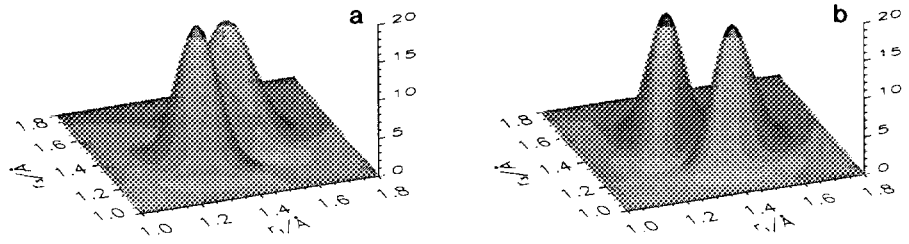

FIG. 7. Probability density (Å^{-2}) functions $\mathcal{P}(r_1, r_3)$ from Eq. (13) for (a) the ν_1 state of lowest energy in the $J = 20$ manifold, $J_{K_aK_c} = 20_{0\,20}$, and (b) the ν_3 state of lowest energy for $J = 20$, $J_{K_aK_c} = 20_{0\,20}$, for $H_2{}^{32}S$.

Figures 8 and 9 give the probability density functions for the (a) A_1 and (b) A_2 MORBID eigenfunctions belonging to the cluster at highest energy in the ν_1/ν_3 state at $J = 30$ and 40, respectively, for $H_2{}^{32}S$. The structures obtained are somewhat similar to those determined for the corresponding wavefunctions of $H_2{}^{80}Se$ (Fig. 11 of Ref. (*10*)), but for $H_2{}^{32}S$, a probability "crater" at the equilibrium geometry is maintained at $J = 30$ and 40. For $H_2{}^{80}Se$, the avoided crossing between the top ν_1/ν_3 cluster and the top $2\nu_2$ cluster takes place at $J = 29$, and the crater is filled at $J = 30$ because of the interaction with $2\nu_2$ basis states. As already described, the analogous crossing is found at $J = 22$ for $H_2{}^{32}S$, and consequently the $J = 30$ and 40 states given here are not significantly influenced by this interaction.

Finally, in Fig. 10 we display the probability density functions for (a) the first primitive cluster state $|\text{PCS } 1\rangle$, and (b) the second primitive cluster state $|\text{PCS } 2\rangle$ belonging to the top cluster in the ν_1/ν_3 state at $J = 40$ for $H_2{}^{32}S$. Even though the $\mathcal{P}(r_1, r_3)$ functions for the MORBID eigenstates at $J = 40$ (Fig. 9) are somewhat different from those obtained at $J = 20$ (Fig. 5), the probability density functions corresponding to the localized wavefunctions at these two J values (Figs. 6 and 10) have highly similar structures.

(d) Average Bond Lengths

We have discussed above that in the primitive cluster states $|\text{PCS}\,j\rangle$, the molecule rotates around one of its bonds. For Type II clusters in the ν_1/ν_3 state, this bond is vibrationally excited, whereas the other one is in its ground state. Since H_2S has an

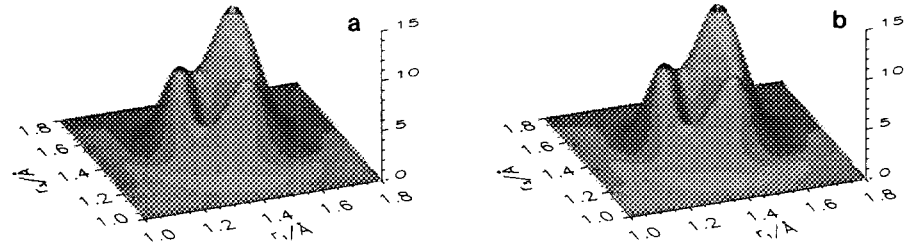

FIG. 8. Probability density (Å^{-2}) functions $\mathcal{P}(r_1, r_3)$ from Eq. (13) for (a) the MORBID eigenfunction with symmetry A_1 and (b) the MORBID eigenfunction with symmetry A_2 belonging to the cluster at highest energy in the ν_1/ν_3 state at $J = 40$ for $H_2{}^{32}S$.

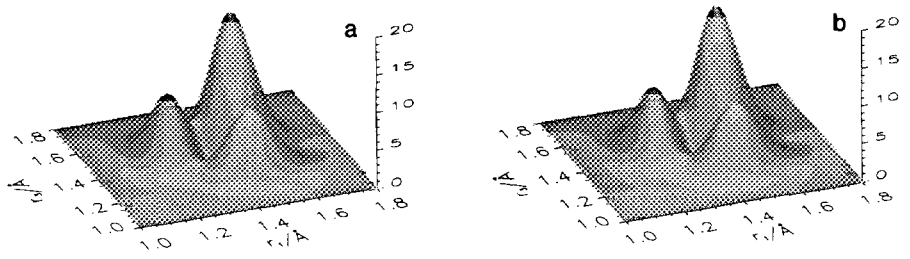

FIG. 9. Probability density ($Å^{-2}$) functions $\mathcal{P}(r_1, r_3)$ from Eq. (13) for (a) the MORBID eigenfunction with symmetry A_1 and (b) the MORBID eigenfunction with symmetry A_2 belonging to the cluster at highest energy in the ν_1/ν_3 state at $J = 40$ for $H_2{}^{32}S$.

equilibrium bond angle close to 90° the bond that does not coincide with the rotation axis is almost perpendicular to this axis. We showed in Ref. (*10*) that for $H_2{}^{80}Se$, this bond lengthens with increasing J because of centrifugal distortion. Table V demonstrates this effect for $H_2{}^{32}S$. The table gives average bond lengths (Eq. (15)) for the $J = 0$ wavefunction in the vibrational ground state and for the primitive cluster states $|\text{PCS } 1\rangle$ representing the $J = 20$ top cluster in the vibrational ground state and in the ν_1/ν_3 vibrational state, respectively. Further, Table V gives average bond lengths for the local mode function $|\psi_+\rangle$ given by

$$|\psi_+\rangle = \frac{1}{\sqrt{2}}(|\nu_1; 0_{00}\rangle + |\nu_3; 0_{00}\rangle), \tag{17}$$

where $|\nu_1; 0_{00}\rangle$ and $|\nu_3; 0_{00}\rangle$ are the MORBID eigenfunctions obtained for $J = 0$ in the ν_1 and ν_3 states, respectively. The function $|\psi_+\rangle$ represents a rotationless, localized excitation of the S–H_3 stretching motion.

For the wavefunction $|\psi_+\rangle$, $\overline{r_1}$ is unchanged relative to the vibrational ground state, but $\overline{r_3}$ is increased by 0.033 Å due to the vibrational excitation. For the first primitive cluster state $|\text{PCS } 1\rangle$ belonging to the "top" cluster in the ν_1/ν_3 vibrational state at $J = 20$, the internuclear distance r_1 is lengthened by $\Delta r_1 = 0.026$ Å, and the distance r_3 is lengthened by $\Delta r_3 = 0.007$ Å relative to the average bond lengths found for the wavefunction $|\psi_+\rangle$. These results are almost equal to the elongations of $(\Delta r_1, \Delta r_3) = (0.024\text{ Å}, 0.009\text{ Å})$ determined for the first primitive cluster state $|\text{PCS } 1\rangle$ for the top cluster in the vibrational ground state at $J = 20$ relative to the $J = 0$ level of

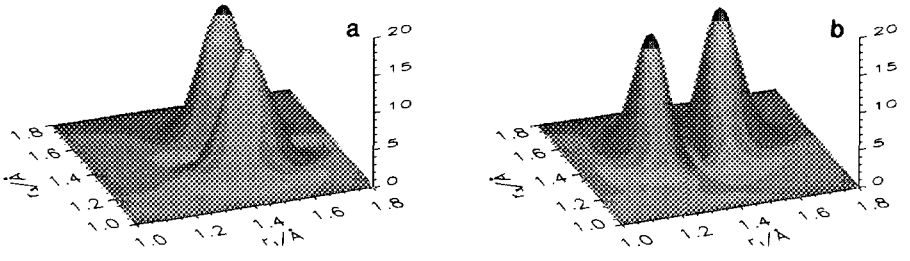

FIG. 10. Probability density ($Å^{-2}$) functions $\mathcal{P}(r_1, r_3)$ from Eq. (13) for (a) the first primitive cluster state $|\text{PCS } 1\rangle$ and (b) the second primitive cluster state $|\text{PCS } 2\rangle$ belonging to the cluster at highest energy in the ν_1/ν_3 state at $J = 40$ for $H_2{}^{32}S$.

TABLE V

Average Bond Length Values Calculated from Eq. (15) for Rotation–Vibration States of $H_2{}^{32}S$

	$J = 0$		$J = 20^a$			
	$\overline{r_1}$/Å	$\overline{r_3}$/Å	$\overline{r_1}$/Å	$\overline{r_3}$/Å	$\Delta\overline{r_1}^b$/Å	$\Delta\overline{r_3}^b$/Å
V. g. s.[c]	1.355	1.355	1.379	1.364	0.024	0.009
ν_1/ν_3[d]	1.355	1.388	1.381	1.395	0.026	0.007

[a] Average bond lengths for the first primitive cluster function |PCS 1⟩ in the "top" cluster.

[b] $\Delta\overline{r_j} = \overline{r_j}(J = 20) - \overline{r_j}(J = 0)$.

[c] Vibrational ground state.

[d] For $J = 0$, the average bond lengths are calculated for the local mode function $|\psi_+\rangle$ given by Eq. (17).

the vibrational ground state. We observe that both in the vibrational ground state and in the ν_1/ν_3 vibrational state, rotational excitation to $J = 20$ causes the S–H_1 bond (r_1), which is approximately perpendicular to the axis of rotation, to lengthen significantly due to centrifugal distortion, whereas the S–H_3 bond (r_3), which lies along the rotation axis, is much less affected.

We can further illustrate this phenomenon by comparing the probability density functions for the primitive cluster states |PCS 1⟩ and |PCS 2⟩ belonging to the top cluster in the ν_1/ν_3 state at $J = 40$ for $H_2{}^{32}S$ (Fig. 10) with the analogous functions for $J = 20$ (Fig. 6). For the function |PCS 1⟩ at $J = 40$, we obtain $\overline{r_1} = 1.464$ Å and $\overline{r_3} = 1.393$ Å, so that the bond lengths are elongated by $(\Delta r_1, \Delta r_3) = (0.109$ Å, 0.005 Å) relative to the average bond lengths found for the wavefunction $|\psi_+\rangle$. Figure 11a shows the result of subtracting the probability density function for the wavefunction |PCS 1⟩ belonging to the top cluster in the ν_1/ν_3 state at $J = 20$ for $H_2{}^{32}S$ (Fig. 6a) from the corresponding function obtained for $J = 40$ (Fig. 10a). Figure 11b shows the analogous difference for the probability density function |PCS 2⟩. It is seen that

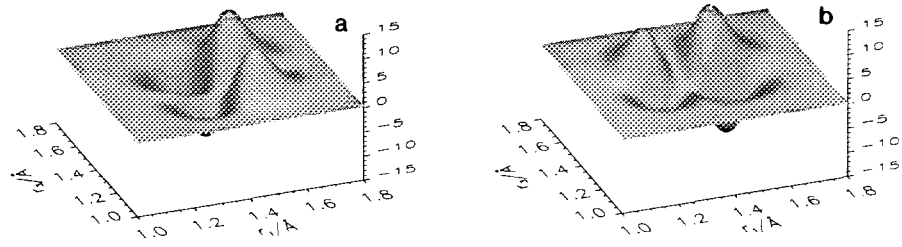

FIG. 11. (a) The difference between the probability density (Å^{-2}) functions for the first primitive cluster state |PCS 1⟩ belonging to the cluster at highest energy in the ν_1/ν_3 state at $J = 40$ (Fig. 10a) and $J = 20$ (Fig. 6a), respectively, for $H_2{}^{32}S$. (b) The difference between the probability density (Å^{-2}) functions for the second primitive cluster state |PCS 2⟩ belonging to the cluster at highest energy in the ν_1/ν_3 state at $J = 40$ (Fig. 10b) and $J = 20$ (Fig. 6b), respectively, for $H_2{}^{32}S$.

for the function $|\text{PCS } 1\rangle$, centrifugal distortion causes a uniform displacement of the probability density function along the r_1 axis when J increases, whereas for $|\text{PCS } 2\rangle$, the probability distribution is displaced along the r_3 axis.

V. SUMMARY AND CONCLUSION

The present paper reports a theoretical investigation of the nearly degenerate, four-member groups of energy levels formed in the rotation–vibration energy spectrum of hydrogen sulfide H_2S. The calculations have been carried out with the MORBID computer program (*11–13*). As the initial step toward the characterization of the fourfold energy clusters we have optimized the parameters in an analytical representation of the potential energy function (Eq. (1)) for the electronic ground state of H_2S on the basis of experimental data. The input data set for this fitting comprised a total of 548 rotation–vibration energy spacings involving $J \leqslant 5$ for the four isotopic molecules $H_2{}^{32}S$, $D_2{}^{32}S$, $HD^{32}S$, and $H_2{}^{34}S$. We adjusted 14 parameters to reproduce the input data with root-mean-square deviations of 0.134 cm^{-1} for the rotational energy spacings and 0.422 cm^{-1} for the vibrational spacings. In the H_2S fitting reported in the present work, we have used almost twice as many input data points as in the analogous fitting carried out previously for the heavier H_2Se molecule (*9*). For both molecules, 14 parameters were optimized. However, the values of the RMS deviations obtained for H_2S are only about 1.5 times larger than those obtained for H_2Se.

We have used the fitted potential energy function as basis for an extensive calculation of the rotation–vibration energy levels in the vibrational ground state, the ν_2 vibrational state, and the $\nu_1/\nu_3/2\nu_2$ interacting vibrational states of $H_2{}^{32}S$ for $J \leqslant 40$. The rotational energy level spectra obtained for these vibrational states of $H_2{}^{32}S$ are highly similar in structure to those calculated previously for $H_2{}^{80}Se$ (*9, 10*), although there is some difference in detail.

We can summarize our analysis of the rotational energy manifolds as follows: For low J values, the rotational energy pattern is essentially given by the energy spectrum of a rigid rotor, but as J increases, we find a substantial deviation from the rigid rotor picture in that fourfold energy clusters form in the upper part of the J multiplets. There are two fundamentally different types of clusters: Type I clusters, which we have calculated in the vibrational ground state and in the ν_2 and $2\nu_2$ states of $H_2{}^{32}S$, involve only one vibrational state. In each cluster state, the molecule carries out a vibrational motion largely identical to that carried out in the $J = 0$ level of the vibrational state in question. Type II clusters are formed by coalescence of rovibrational energy doublets belonging to two stretching vibrational states with different symmetries. We have calculated Type II cluster energies and wavefunctions for the ν_1 and ν_3 vibrational states of $H_2{}^{32}S$. In a Type II cluster state, the stretching vibrational motion is radically different from the motion carried out for $J = 0$ in the vibrational states involved. Our analysis of the Type II cluster wavefunctions obtained for the ν_1/ν_3 vibrational state offers a simple picture of the motion associated with them: The stretching excitation is localized in one bond, and the molecule rotates around this bond. The other bond, which is almost perpendicular to the rotation axis, is lengthened due to centrifugal distortion.

Comparison between the results of the present work and those of Refs. (*9, 10*) shows that the rovibrational energy spectrum of H_2S is extremely similar in structure to that of H_2Se. This is obviously due to the similarity between the potential energy functions of these two molecules and to the fact that for both molecules, the mass of

the central nucleus can, to a good approximation, be considered infinitely large in comparison with the masses of the "end" H nuclei. Hence it is very probable that at the "heavy" end of the H_2X "family," e.g., for H_2Te, analogous cluster formation will be found. From Eq. (8), we calculate $J_{CR} = 8$ for the most abundant H_2Te isotopomer, $H_2{}^{130}Te$, using as input the rotational constants from Ref. (*45*) and the bending fundamental energy from Ref. (*46*). As described in Section III, semiclassical theory predicts the qualitative deviation of the rotational energies from the customary rigid rotor picture to become apparent at $J = J_{CR}$, and the low J_{CR} value found for H_2Te (the corresponding values for H_2Se and H_2S are 12 and 15, respectively) indicates that for this molecule, clusters are found at low J values readily accessible to experimental spectroscopy. It is still an open question whether the cluster effects are present in the lighter H_2O molecule. If the rovibrational energies of the water molecule form clusters, the clusters appear at very high J and K values. The corresponding quantum states are hardly accessible to present-day experimental techniques, and their energies are difficult to calculate with methods such as MORBID due to the sizes of the Hamiltonian matrices involved. From the results of the present work and those of Refs. (*9, 10*) we can conclude, however, that in order to determine the high J, high K asymptotic behavior of the H_2O rovibrational energies by theoretical calculations, it is necessary to use theoretical methods which account explicitly for all motions of the molecule, and it is necessary to base the calculations on very accurate potential energy surfaces.

ACKNOWLEDGMENTS

We are grateful to J.-M. Flaud for supplying us with unpublished term values for D_2S and HDS, to W. J. Lafferty for helping us access Refs. (*14, 16*), and to K. K. Lehmann for alerting us to the existence of Ref. (*8*). This work was supported by Deutsche Forschungsgemeinschaft Grant Je 144/2-3 and by the Fonds der Chemischen Industrie. P.J. acknowledges further support from the Dr. Otto Röhm Gedächtnisstiftung and from the Fritz Thyssen-Stiftung. The present work has been possible only through the use of two supercomputers made available to us by the State of Hessen: the Siemens/Nixdorf S400/40 installation at the Technical University Darmstadt and the Siemens/Nixdorf S100/10 installation at the Justus Liebig University Giessen. The major part of the calculations reported here was carried out on these installations, and we are grateful for generous allotments of computer time. I.N.K. is grateful to the Institute of Physical Chemistry at the Justus Liebig University Giessen, and particularly to B. P. Winnewisser and M. Winnewisser, for hospitality. We thank P. R. Bunker and J. K. G. Watson for critically reading the manuscript and suggesting improvements.

RECEIVED: September 20, 1993

REFERENCES

1. I. N. KOZIN, S. P. BELOV, O. L. POLYANSKY, AND M. YU. TRETYAKOV, *J. Mol. Spectrosc.* **152,** 13–28 (1992).
2. I. N. KOZIN, O. L. POLYANSKY, S. I. PRIPOLZIN, AND V. L. VAKS, *J. Mol. Spectrosc.* **156,** 504–506 (1992).
3. I. N. KOZIN, S. KLEE, P. JENSEN, O. L. POLYANSKY, AND I. M. PAVLICHENKOV, *J. Mol. Spectrosc.* **158,** 409–422 (1993).
4. B. I. ZHILINSKII AND I. M. PAVLICHENKOV, *Opt. Spectrosc. (USSR)* **64,** 688–690 (1988). [In Russian]
5. J. MAKAREWICZ AND J. PYKA, *Mol. Phys.* **68,** 107–127 (1989).
6. J. MAKAREWICZ, *Mol. Phys.* **69,** 903–921 (1990).
7. J. PYKA, *Mol. Phys.* **70,** 547–561 (1990).
8. K. K. LEHMANN, *J. Chem. Phys.* **95,** 2361–2370 (1991).
9. P. JENSEN AND I. N. KOZIN, *J. Mol. Spectrosc.* **160,** 39–57 (1993).

10. I. N. KOZIN AND P. JENSEN, *J. Mol. Spectrosc.* **161,** 186–207 (1993).
11. P. JENSEN, *J. Mol. Spectrosc.* **128,** 478–501 (1988).
12. P. JENSEN, *J. Chem. Soc. Faraday Trans. 2* **84,** 1315–1340 (1988).
13. P. JENSEN, *in* "Methods in Computational Molecular Physics" (S. Wilson and G. H. F. Diercksen, Eds.), Plenum, New York, 1992.
14. H. C. ALLEN, R. E. NAYLOR, AND E. K. PLYLER, *J. Res. Natl. Bur. Stand.* **53,** 321–323 (1954).
15. H. C. ALLEN AND E. K. PLYLER, *J. Chem. Phys.* **25,** 1132–1136 (1956).
16. H. C. ALLEN, E. K. PLYLER, AND L. R. BLAINE, *J. Res. Natl. Bur. Stand.* **59,** 211–214 (1957).
17. M. T. EMERSON AND D. F. EGGERS, JR., *J. Chem. Phys.* **37,** 251–259 (1962).
18. C. HUISZOON AND A. DYMANUS, *Physica* **31,** 1049–1052 (1965).
19. R. E. MILLER, G. E. LEROI, AND D. F. EGGERS, JR., *J. Chem. Phys.* **46,** 2292–2297 (1967).
20. T. H. EDWARDS, N. K. MONCUR, AND L. E. SNYDER, *J. Chem. Phys.* **46,** 2139–2142 (1967).
21. R. E. MILLER, G. E. LEROI, AND T. M. HARD, *J. Chem. Phys.* **50,** 677–684 (1969).
22. L. E. SNYDER AND T. H. EDWARDS, *J. Mol. Spectrosc.* **31,** 347–361 (1969).
23. R. L. COOK, F. C. DE LUCIA, AND P. HELMINGER, *J. Mol. Spectrosc.* **41,** 123–136 (1972).
24. P. HELMINGER, R. L. COOK, AND F. C. DE LUCIA, *J. Chem. Phys.* **56,** 4581–4584 (1972).
25. R. L. COOK, F. C. DE LUCIA, AND P. HELMINGER, *J. Mol. Struct.* **28,** 237–246 (1975).
26. J. R. GILLIS AND T. H. EDWARDS, *J. Mol. Spectrosc.* **85,** 55–73 (1981).
27. W. C. LANE, T. H. EDWARDS, J. R. GILLIS, F. S. BONOMO, AND F. J. MURCRAY, *J. Mol. Spectrosc.* **95,** 365–380 (1982).
28. J.-M. FLAUD, C. CAMY-PEYRET, AND J. W. C. JOHNS, *Can. J. Phys.* **61,** 1462–1473 (1983).
29. L. L. STROW, *J. Mol. Spectrosc.* **97,** 9–28 (1983).
30. L. L. STROW, *J. Quant. Spectrosc. Radiat. Transfer* **29,** 395–406 (1983).
31. P. POKROWSKY, *Appl. Opt.* **22,** 2221–2223 (1983).
32. L. LECHUGA-FOSSAT, J.-M. FLAUD, C. CAMY-PEYRET, AND J. W. C. JOHNS, *Can. J. Phys.* **62,** 1889–1923 (1984).
33. J. R. GILLIS, R. D. BLATHERWICK, AND F. S. BONOMO, *J. Mol. Spectrosc.* **114,** 228–233 (1985).
34. C. CAMY-PEYRET, J.-M. FLAUD, L. LECHUGA-FOSSAT, AND J. W. C. JOHNS, *J. Mol. Spectrosc.* **109,** 300–333 (1985).
35. W. C. LANE, T. H. EDWARDS, J. R. GILLIS, F. S. BONOMO, AND F. J. MURCRAY, *J. Mol. Spectrosc.* **111,** 320–326 (1985).
36. L. LECHUGA-FOSSAT, J.-M. FLAUD, C. CAMY-PEYRET, P. ARCAS, AND M. CUISENIER, *Mol. Phys.* **61,** 23–32 (1987).
37. C. CAMY-PEYRET, J.-M. FLAUD, A. N'GOM, AND J. W. C. JOHNS, *Mol. Phys.* **65,** 649–657 (1988).
38. J.-M. FLAUD, private communication (1993).
39. P. JENSEN, *J. Mol. Spectrosc.* **133,** 438–460 (1989).
40. E. KAUPPI AND L. HALONEN, *J. Phys. Chem.* **94,** 5779–5785 (1990).
41. J. SENEKOWITSCH, S. CARTER, A. ZILCH, H.-J. WERNER, N. C. HANDY, AND P. ROSMUS, *J. Chem. Phys.* **90,** 783–794 (1990).
42. I. M. MILLS AND A. G. ROBIETTE, *Mol. Phys.* **56,** 743–765 (1985).
43. L. HALONEN AND T. CARRINGTON, JR., *J. Chem. Phys.* **88,** 4171–4185 (1988).
44. P. R. BUNKER, "Molecular Symmetry and Spectroscopy," Academic Press, London, 1979.
45. A. V. BURENIN, A. F. KRUPNOV, S. V. MART'YANOV, A. A. MEL'NIKOV, AND L. I. NIKOLAYEV, *J. Mol. Spectrosc.* **75,** 333–337 (1979).
46. R. A. HILL, T. H. EDWARDS, K. ROSSMANN, K. NARAHARI RAO, AND H. H. NIELSEN, *J. Mol. Spectrosc.* **14,** 221–243 (1964).